UNIVERSITY OF CALIFORNIA, BERKELEY
Department of Materials Sciences and Mineral Engineering

First Annual Report

to

U.S. Air Force Office of Scientific Research

on

MICROMECHANISMS OF MONOTONIC AND CYCLIC SUBCRITICAL CRACK GROWTH IN ADVANCED HIGH MELTING POINT LOW-DUCTILITY INTERMETALLICS

Grant No. AFOSR-90-0167
for period 15 April 1990 to 14 April 1991

by

K. T. Venkateswara Rao, L. Murugesh, L. C. DeJonghe
and R. O. Ritchie

May 1991

Report No. UCB/R/91/A1072

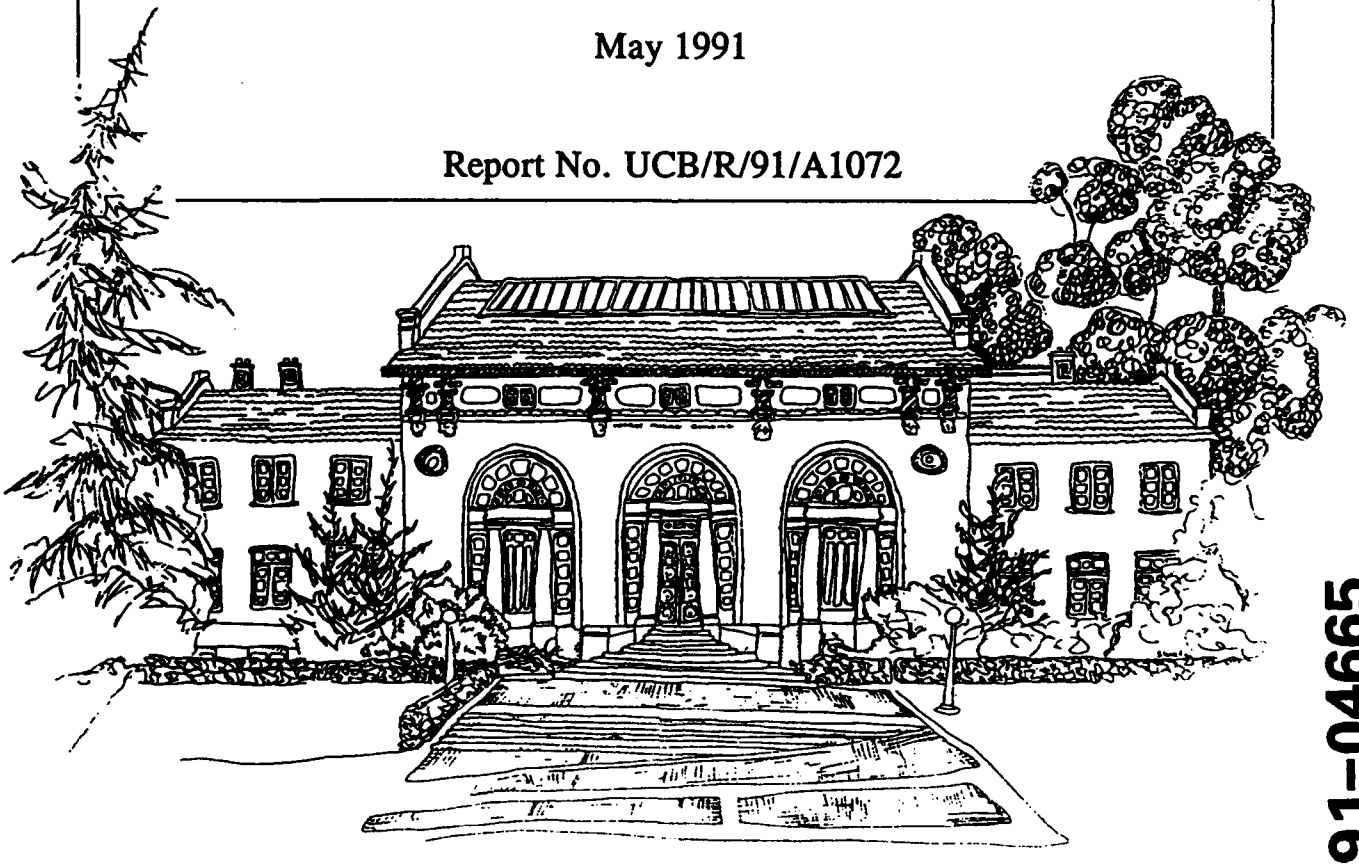

Hearst Mining Building, Berkeley, CA 94720

UNCLASSIFIED
SECURITY CLASSIFICATION OF THIS PAGE

REPORT DOCUMENTATION PAGE

1a. REPORT SECURITY CLASSIFICATION Unclassified	1b. RESTRICTIVE MARKINGS None
2a. SECURITY CLASSIFICATION AUTHORITY Not Applicable	3. DISTRIBUTION / AVAILABILITY OF REPORT ~~Not Applicable~~ unlimited
2b. DECLASSIFICATION / DOWNGRADING SCHEDULE Not Applicable	
4. PERFORMING ORGANIZATION REPORT NUMBER(S) UCB/R/91/A1072	5. MONITORING ORGANIZATION REPORT NUMBER(S)
6a. NAME OF PERFORMING ORGANIZATION Robert O. Ritchie, Dept. of Mat. Sci. & Minl. Eng. 6b. OFFICE SYMBOL (If applicable)	7a. NAME OF MONITORING ORGANIZATION Air Force Office of Scientific Research AFOSR/NE
6c. ADDRESS (City, State, and ZIP Code) University of California Hearst Mining Building Berkeley, California 94720	7b. ADDRESS (City, State, and ZIP Code) Bldg. 410, Bolling AFB Washington, D.C. 20322 ATTN: Dr. A. H. Rosenstein, AFOSR/NE
8a. NAME OF FUNDING / SPONSORING ORGANIZATION Same as 7a 8b. OFFICE SYMBOL (If applicable)	9. PROCUREMENT INSTRUMENT IDENTIFICATION NUMBER AFOSR-90-0167
8c. ADDRESS (City, State, and ZIP Code) Same as 7b	10. SOURCE OF FUNDING NUMBERS PROGRAM ELEMENT NO. 61102 / PROJECT NO. 2306 / TASK NO. A1 / WORK UNIT ACCESSION NO.

11. TITLE (Include Security Classification)
MICROMECHANISMS OF MONOTONIC AND CYCLIC SUBCRITICAL CRACK GROWTH IN ADVANCED HIGH MELTING POINT LOW-DUCTILITY INTERMETALLICS (Unclassified)

12. PERSONAL AUTHOR(S)
VENKATESWARA RAO, K.T., MURUGESH, L., DeJONGHE, L.C. and RITCHIE, R.O.

13a. TYPE OF REPORT	13b. TIME COVERED	14. DATE OF REPORT (Year, Month, Day)	15. PAGE COUNT
Annual	FROM 90/4/15 TO 91/4/14	1991 May 1	

16. SUPPLEMENTARY NOTATION

17. COSATI CODES			18. SUBJECT TERMS (Continue on reverse if necessary and identify by block number)
FIELD	GROUP	SUB-GROUP	Intermetallic Composites; Fatigue Crack Propagation; Fracture Toughness

19. ABSTRACT (Continue on reverse if necessary and identify by block number)

The next generation of high-performance jet engines will require markedly stiffer materials, operating at higher stress levels and capable of withstanding temperatures of up to 1650°C. Prime candidates for such applications include ordered intermetallics, ceramics and composites based on metal, intermetallic and ceramic or carbon matrices, all of which are currently of limited use due to their low ductility and fracture properties. Moreover, there is a lack of fundamental understanding on the micromechanisms influencing crack growth in these materials, particularly intermetallics. Accordingly, the present study is aimed at exploring the potential of intermetallic alloys and their composites as advanced structural materials by identifying the critical factors influencing the crack-propagation resistance under monotonic and cyclic ~~loading conditions~~ loads.

(cover)

20. DISTRIBUTION / AVAILABILITY OF ABSTRACT	21. ABSTRACT SECURITY CLASSIFICATION
☒ UNCLASSIFIED/UNLIMITED ☐ SAME AS RPT. ☐ DTIC USERS	Unclassified
22a. NAME OF RESPONSIBLE INDIVIDUAL ~~Robert O. Ritchie~~ Rosenstein	22b. TELEPHONE (Include Area Code) ~~(415) 642-0417~~ 202-767-4933 / 22c. OFFICE SYMBOL NE

DD FORM 1473, 84 MAR 83 APR edition may be used until exhausted. All other editions are obsolete.

SECURITY CLASSIFICATION OF THIS PAGE
Unclassified

(A)

(cont'd)

During the first year of this program, attention is focused on the Nb_3Al and TiAl intermetallic systems. In both cases, the principal mechanism of toughening is to impede crack advance from crack bridging by ductile second phase particles. Reactive sintering and vacuum hot pressing techniques are successful in processing Nb_3Al intermetallics and duplex Nb/Nb_3Al microstructures with a stringy Nb phase can be achieved through thermal treatments. Characterization of the mechanical properties will commence in the second year.

niobium

With respect to TiAl, the role of ductile-phase toughening is compared under monotonic and cyclic loading, specifically involving the fracture and fatigue-crack growth behavior in a γ-TiAl intermetallic alloy reinforced with 10 vol.% of ~50 μm-sized ductile TiNb particles. Under monotonic loading, substantial toughening is achieved in the composite primarily from crack bridging by uncracked TiNb particles in the crack wake. Compared to the K_{Ic} value of ~8 MPa$\sqrt{m}$ for monolithic TiAl, the composite shows significant resistance-curve behavior with steady-state toughness exceeding 25 MPa$\sqrt{m}$; in this regime, measured bridging zones approach ~4 mm in length. The highlight of the first year's work is the fact that, in contrast to behavior under monotonic loading, such ductile-particle toughening is found to be far less effective under cyclic loading due to the susceptibility of the ductile metallic phase to fatigue failure. No evidence of crack bridging by TiNb particles is observed to within ~150 μm of the crack tip, and fatigue-crack propagation is observed at stress-intensity levels as low as 6 MPa$\sqrt{m}$, far below those required to initiate cracking under monotonic loading.

Report No. UCB/R/91/A1072

First Annual Report

to

U.S. Air Force Office of Scientific Research

on

MICROMECHANISMS OF MONOTONIC AND CYCLIC SUBCRITICAL CRACK GROWTH IN ADVANCED HIGH MELTING POINT LOW-DUCTILITY INTERMETALLICS

Grant No. AFOSR-90-0167

for period 15 April 1990 to 14 April 1991

submitted to

U.S. Air Force Office of Scientific Research
Bldg. 410, Bolling Air Force Base
Washington, D.C. 20322
Attention: Dr. Alan H. Rosenstein

submitted by

K. T. Venkateswara Rao, L. Murugesh, L. C. De Jonghe and R. O. Ritchie
Department of Materials Science and Mineral Engineering
University of California
Berkeley, California 94720

May 1991

TABLE OF CONTENTS

MICROMECHANISMS OF MONOTONIC AND CYCLIC SUBCRITICAL CRACK GROWTH IN ADVANCED HIGH MELTING POINT LOW-DUCTILITY INTERMETALLICS

K. T. Venkateswara Rao, L. Murugesh, L. C. De Jonghe and R. O. Ritchie

(Grant No. AFOSR-90-0167)

FOREWORD

This manuscript constitutes the First Annual Report on Grant No. AFOSR-90-0167, administered by the U.S. Air Force Office of Scientific Research, with Dr. Alan H. Rosenstein as program manager. The work, covering the period April 15, 1990, through April 14, 1991, was performed under the direction of Dr. R. O. Ritchie, Professor of Materials Science, University of California at Berkeley, and Dr. L. C. De Jonghe, Professor of Materials Science, University of California at Berkeley, with Dr. K. T. Venkateswara Rao as Research Engineer, L. Murugesh as graduate student, and D. Nath and J. C. McNulty as undergraduate engineering aides.

ABSTRACT

The next generation of high-performance jet engines will require markedly stiffer materials, operating at higher stress levels and capable of withstanding temperatures of up to 1650°C. Prime candidates for such applications include ordered intermetallics, ceramics and composites based on metal, intermetallic and ceramic or carbon matrices, all of which are currently of limited use due to their low ductility and fracture properties. Moreover, there is a lack of fundamental understanding on the micromechanisms influencing crack growth in these materials, particularly intermetallics. Accordingly, the present study is aimed at exploring the potential of intermetallic alloys and their composites as advanced structural materials by identifying the critical factors influencing the crack-propagation resistance under monotonic and cyclic loading conditions.

During the first year of this program, attention is focused on the Nb_3Al and TiAl intermetallic systems. In both cases, the principal mechanism of toughening is to impede crack advance from crack bridging by ductile second phase particles. Reactive sintering and vacuum hot pressing techniques are successful in processing Nb_3Al intermetallics and duplex Nb/Nb_3Al microstructures with a stringy Nb phase can be achieved through thermal treatments. Characterization of the mechanical properties will commence in the second year.

With respect to TiAl, the role of ductile-phase toughening is compared under monotonic and cyclic loading, specifically involving the fracture and fatigue-crack growth behavior in a γ-TiAl intermetallic alloy reinforced with 10 vol.% of $\sim$50 μm-sized ductile TiNb particles. Under monotonic loading, substantial toughening is achieved in the composite primarily from crack bridging by uncracked TiNb particles in the crack wake. Compared to the K_{Ic} value of $\sim$8 MPa$\sqrt{m}$ for monolithic TiAl, the composite shows significant resistance-curve behavior with steady-state toughness exceeding 25 MPa$\sqrt{m}$; in this regime, measured bridging zones approach $\sim$4 mm in length. The highlight of the first year's work is the fact that, in contrast to behavior under monotonic loading, such ductile-particle toughening is found to be far less effective under cyclic loading due to the susceptibility of the ductile metallic phase to fatigue failure. No evidence of crack bridging by TiNb particles is observed to within $\sim$150 μm of the crack tip, and fatigue-crack propagation is observed at stress-intensity levels as low as 6 MPa$\sqrt{m}$, far below those required to initiate cracking under monotonic loading.

1. INTRODUCTION

Current gas-turbine engines in commercial use primarily utilize nickel-base superalloys in the hot turbine and compressor sections and primarily nickel-base and titanium alloys in the cooler compressor sections. However, since the efficiency and total thrust of a jet engine is a direct function of the peak temperature of the working fluid and current limits are set by thermal constraints on materials, these alloys are unlikely to meet the performance needs of the next generation of engines, which will require markedly stiffer materials operating at high stress levels at very much higher temperatures [1]. At present, materials are being sought which can operate at temperatures as high as 1650°C, although materials which can operate effectively at 1000°C would represent significant progress. Prime candidates include ordered intermetallics, ceramics and composites based on metal, intermetallic, ceramic or carbon matrices, all materials which suffer from potential problems of very low ductility, fracture toughness, and subcritical crack-growth resistance [2,3].

Much progress has been achieved over the past few years in the understanding of the mechanical, thermal and environmental behavior of such advanced high-temperature materials; however, the most significant void in this understanding still pertains to their fracture, fatigue and creep properties. Cyclic fatigue in particular has been largely overlooked, based on the widely held perception that low-ductility materials may in fact be largely immune to fatigue failure [4]. The refuted existence of a true cyclic fatigue phenomenon in these materials has been based largely on limited crack-tip plasticity. However, other inelastic deformation mechanisms, such as microcracking, phase transformation, reinforcement-phase deformation or frictional sliding between the phase and the matrix, may exist in the vicinity of the crack. In fact, recent studies by one of the authors [5-7], and others [8-11], have shown that premature fatigue failures can readily occur in ceramic and graphite/carbon materials with toughnesses as low as 1-2 $MPa\sqrt{m}$. In light of the service conditions that such intermetallic and ceramic alloys may see in future engines, it is clear that the generation of information on fatigue lifetimes and cyclic crack-growth resistance in these alloys must be regarded as extremely important; moreover, a mechanistic understanding of the primary mechanical, microstructural and environmental factors that contribute to their fracture toughness and cyclic fatigue-crack growth properties is of even greater significance.

Accordingly, the principal objective of this study is to seek a fundamental understanding of the mechanics and micromechanisms of ambient and elevated temperature fracture-toughness and cyclic fatigue-crack propagation behavior in advanced, low-ductility intermetallic alloys. Specifically, it is planned to examine the underlying basis for crack-growth resistance under monotonic and cyclic loads, at ambient temperatures and up to and

exceeding 1000°C, in several model intermetallics in both monolithic and composite form. Initial candidate materials include niobium aluminides (Nb_3Al, Nb_2Al) and niobium silicides (Nb_5Si_3, $NbSi_2$), which will be synthesized in-house, TiNb-reinforced γ-TiAl intermetallics processed at Pratt and Whitney, and molybdenum disilicides ($MoSi_2$) in both unreinforced and with SiC-whisker reinforcement, which have been obtained from Los Alamos National Laboratory, United Technologies and McDonnell-Douglas. To our knowledge, no cyclic crack-growth data have ever been obtained in the past for such materials. The study is focused on integrating the processing and properties of such advanced low-ductility alloys and will explore the effect on properties, and the difficulty of the synthesizing, of brittle fiber/whisker and ductile-particle reinforcements, using unique processing and mechanical fatigue-testing techniques. The ultimate aim is to provide guidelines for the alloy design of new microstructures in hybrid intermetallic systems with superior resistance to incipient crack growth under both sustained and alternating loads.

This report covers the first year of the program of research where attention has been focused on the fatigue-crack propagation resistance of ductile-phase toughened TiNb/γ-TiAl intermetallic-matrix composites and the processing of dual-phase Nb_3Al-Nb microstructures. Specifically, the role of ductile TiNb particles on crack-growth in the TiNb/TiAl composite is contrasted under monotonic vs. cyclic loading conditions. In addition, Nb_3Al-Nb *in situ* composites have been successfully processed by vacuum hot-pressing and reactive sintering techniques and the microstructures modified through thermal treatments to obtain filamentary Nb in an Nb_3Al matrix. Ongoing research work on the micromechanisms of fracture and fatigue-crack propagation in $MoSi_2$/Nb, $MoSi_2$/SiC composites is also briefly discussed.

1.1 References

1) J. J. de Luccia, R. E. Trabocco and J. F. Collins, *Adv. Mat. Proc.* **136**:5, 39 (1989).

2) J. D. Destefani, *ibid.* **136**:2, 37 (1989).

3) R. H. Jeal, *Met. Matls.* **5**, 539 (1989).

4) A. G. Evans, *Int. J. Fract.* **16**, 485 (1980).

5) R. H. Dauskardt, W. Yu and R. O. Ritchie, *J. Am. Ceram. Soc.* **70**, C-248 (1987).

6) R. H. Dauskardt and R. O. Ritchie, *Closed Loop* **7**, 7 (1989).

7) R. O. Ritchie, R. H. Dauskardt, W. Yu and A. M. Brendzel, *J. Biomed. Mat. Res.* **27**, 189 (1990).

8) L. Ewart and S. Suresh, *J. Mater. Sci. Lett.* **5**, 774 (1986).

9) S. Suresh, L. X. Han and J. P. Petrovic, *J. Am. Ceram. Soc.* **71**, C-158 (1988).

10) K. J. Bowman, P. E. Reyes-Marel and I.-W. Chen, in *Advanced Structural Ceramics*, MRS Symp. Proc., P. F. Becher et al. (eds.), MRS, Pittsburgh, PA (1986).

11) M. J. Reece, F. Guiu and M. F. R. Sammur, *J. Am. Ceram. Soc.* **72**, 348 (1989).

2. ROLE OF DUCTILE-PHASE REINFORCEMENTS ON THE FATIGUE AND FRACTURE BEHAVIOR OF TiNb/γ-TiAl INTERMETALLIC COMPOSITES

2.1 Introduction

Structural alloys based on the ordered intermetallic compounds TiAl, Ti_3Al, Ni_3Al, NiAl and $MoSi_2$ have recently become potential candidate materials for several advanced high-temperature aerospace applications, primarily because of their high specific strength and stiffness which is retained at elevated temperatures exceeding 1000°C [1-5]. Their structural use, however, is currently limited severely by low room-temperature ductility and toughness properties; in fact, measured fracture strains under uniaxial tension can be as low as 1% with fracture toughnesses below ~10 MPa$\sqrt{m}$. Accordingly, much effort has centered on enhancing the ductility and toughness of these materials, both intrinsically and by composite toughening through the incorporation of a reinforcement phase [6-12].

One approach to toughening brittle intermetallics that has attracted considerable recent attention is through the incorporation of ductile-phase reinforcements. Provided the crack path intercepts the reinforcing phase, the dominant contribution to toughening arises from tractions produced by the unbroken, ductile ligaments bridging the two crack surfaces, thus partially shielding the crack tip from remote loads. In addition, crack-tip shielding contributions from crack deflection, crack trapping, crack renucleation and decohesion along the particle/matrix interface can further accentuate this effect. The extent of toughening depends on the length of the bridging zone in the wake of the crack tip; at steady-state, where the zone is at a maximum length governed by ductile-ligament rupture at a critical crack-opening displacement u^*, the steady-state fracture energy increase, ΔG_c, has been estimated in terms of the area fraction f of ductile ligaments intersecting the crack path, their uniaxial yield strength, σ_y, and a representative cross-sectional radius, r, as [13]:

$$\Delta G_c = f \sigma_y r \chi, \tag{2.1}$$

where χ is a dimensionless function representing the work of rupture, given by [13]:

$$\chi = \int_0^{u^*} \frac{\sigma(u)\, du}{\sigma_y \cdot r} \tag{2.2}$$

and can vary between ~0.5 and ~8, depending upon the degree of interface debonding and

constitutive properties of the reinforcement phase [11-14]. Note that this formulation only applies when the size of the bridging zone is small compared to the crack length and specimen dimensions, viz. small-scale bridging.

Several examples of ductile-particle toughened systems can be found in the ceramics literature, where toughness increases by as much as 400% have been reported for Al-reinforced Al_2O_3, Al-reinforced glass, Ni Fe or Co-reinforced MgO, and Co-reinforced WC [15-18]. More recently, such techniques have been successfully employed to toughen intermetallics as well, including γ-TiAl reinforced with Nb or Ti-6Al-4V [10], Nb-reinforced $MoSi_2$ [19] and Nb-reinforced niobium silicide [20].

To date, studies on the mechanical properties of such ductile-particle reinforced brittle materials [10-20] have focused on strength and fracture-toughness behavior, in particular on the contributions to toughening under monotonic loading conditions. In general, high toughness and steep resistance-curve (R-curve) behavior have been obtained where the ductile particles intersecting the crack path *remain unbroken* over significant dimensions (the bridging zone) behind the crack tip. Optimal steady-state properties have been predicted for large values of χ ($\sim$8), for reinforcing phases that work-harden substantially and matrix/reinforcement interfaces that debond readily. Steep resistance curves result from strong particles which do not debond even if they have limited intrinsic ductility; in fact, in such instances debonding is considered undesirable [11,12]. However, despite significant progress in the understanding of toughening in such composites, there have been no corresponding studies to date on how these materials respond to cyclic loading. Moreover, there is some concern over the effectiveness of such bridging mechanisms during fatigue-crack growth, especially since the ductile-metallic ligaments can be susceptible to fatigue failure.

It is therefore the objective of the present work to examine the role of the ductile phase during fatigue-crack propagation in a γ-TiAl intermetallic reinforced with pan-cake shaped TiNb particles, and compare the results with corresponding behavior under monotonic loading.

2.2 Experimental Procedures

Materials: The material under study was a γ-TiAl (Ti-50.5 at.%Al) intermetallic-matrix composite reinforced with $\sim$10 vol.% of ductile (uncoated) single-phase ß-TiNb (Ti-33 at.%Nb), fabricated by hot-pressing the γ-TiAl powder blended with TiNb particles to full consolidation under vaccum at 1025 $\pm$ 15°C and 235 MPa pressure. The billets were then hot forged at 1025 $\pm$ 15°C, deforming the TiNb particles into thin disks. The resulting microstructure (Fig. 2.1a) consisted of pan-cake shaped regions of TiNb, $\sim$50 μm thick (t), $\sim$500 μm in diameter (d) and irregularly spaced $\sim$100-200 μm apart (s), within a matrix of

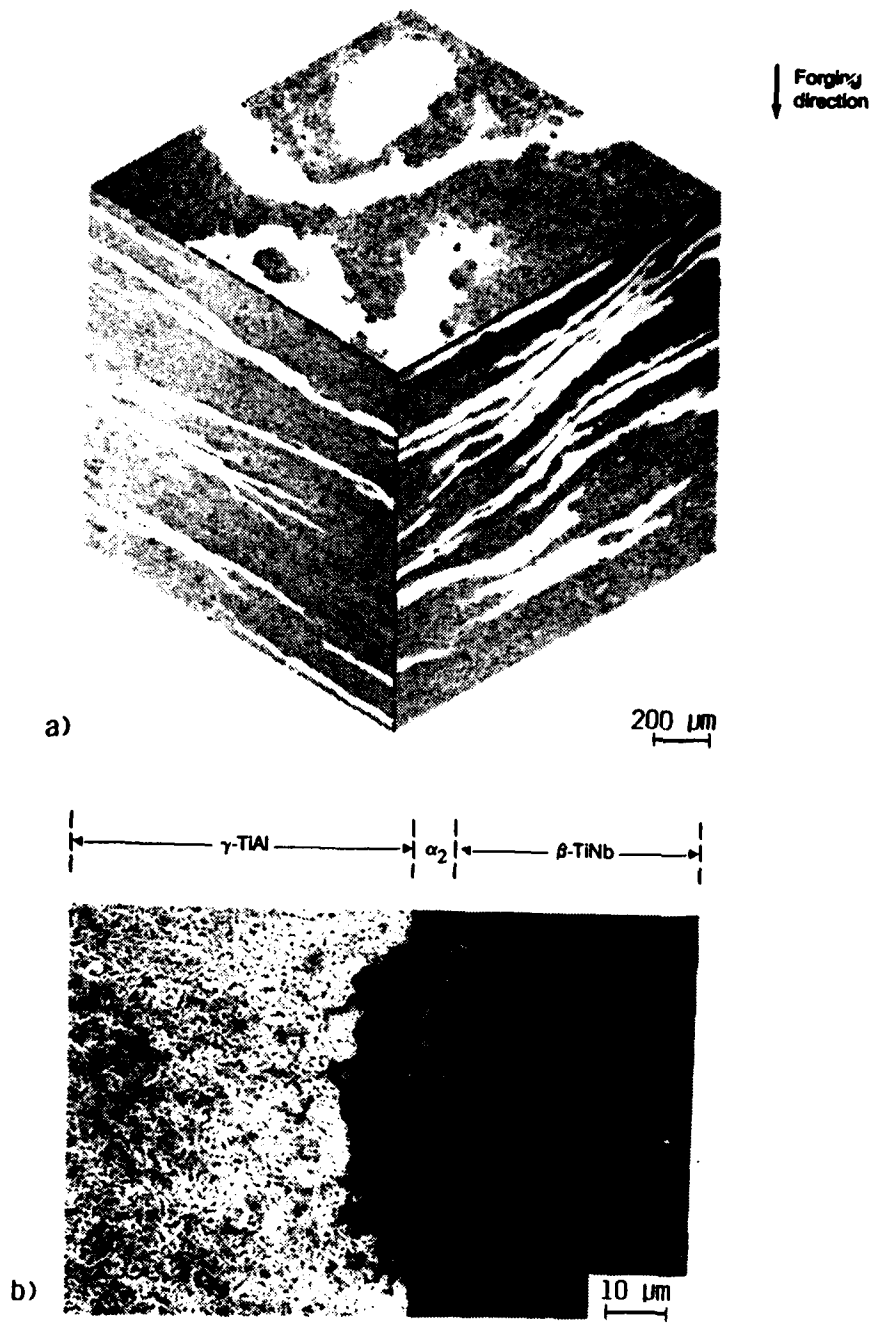

Fig. 2.1: (a) Three dimensional optical micrograph of microstructures in a γ-TiAl intermetallic reinforced with 10 vol.% of ductile TiNb particles, and (b) SEM image of the reaction layer between γ-TiAl matrix and ß-TiNb. Note the pan-cake shaped morphology of the TiNb particles, ~50 µm thick normal to the forging direction.

primarily γ-TiAl (ordered tetragonal $L1_0$ structure) with limited regions of α_2-Ti_3Al (ordered hexagonal DO_{19} structure). At room temperature, typical yield and tensile strengths for monolithic γ-TiAl are between 300-350 MPa with an elongation of ~1.8% [5]; single-phase Ti-33 at.%Nb, conversely, has a yield strength of 430 MPa with negligible work hardening, leading to highly localized plastic deformation and nominal ductility values which are highly dependent on specimen geometry [11,12]. Some degree of interfacial reaction was observed between the TiNb reinforcement and the matrix, resulting in the formation of ~8 μm thick layer of predominantly α_2 (Fig. 2.1b).

Fracture-Toughness Testing: Fracture-toughness behavior of the intermetallic-matrix composite was characterized by determining R-curves in terms of the crack-growth resistance, K_R, as a function of crack extension Δa. Tests were performed in room-temperature air (~22°C and ~45% relative humidity) by monotonically loading precracked, 2.5 mm-thick, single-edged notched bend SEN(B) samples (span L ~ 60 mm and width W ~ 15 mm) in three-point bending [21]. Precracking was carried out by initiating stable crack growth from an electro-discharge machined chevron notch at slow loading rates under displacement control, and subsequently grinding away the crack wake to less than ~200 μm of the crack front to remove any associated bridging zone [10]. Crack lengths were continuously monitored optically using two high-resolution microscopes and a video camera system. Properties in the C-R or edge orientation (pancake faces are parallel to the specimen plane) as well as the C-L or face orientation (crack plane is normal to pancake faces) of the forged billet were examined (Fig. 2.2).

Fatigue Testing: Corresponding fatigue-crack growth behavior under cyclic tension-tension loading was studied using 25 mm-wide and 2.5 mm-thick compact-tension C(T) samples, with a wedge-shaped starter notch to facilitate fatigue precracking. Tests were performed under automated stress-intensity (K) control using exponential load-shedding schemes with a normalized K-gradient of -0.1 mm^{-1}; crack-growth rates (da/dN) were obtained over the range ~10^{-6} and 10^{-12} m/cycle, approaching a threshold stress-intensity range (ΔK_{TH}) below which cracks are presumed dormant. Specimens in the edge (C-R) orientation were cycled at a load ratio ($R = K_{min}/K_{max}$) of 0.1 and a frequency of 50 Hz (sine wave), with crack lengths continuously monitored to a resolution better than 5 μm by measuring the electrical-resistance of thin metal foils bonded onto the specimen surface. Testing procedures are similar to those developed for cyclic fatigue testing of ceramics, as detailed in ref. 22.

Fracture surfaces were examined in the scanning electron microscope (SEM). In addition, metallographically polished sections of the crack paths, both perpendicular and

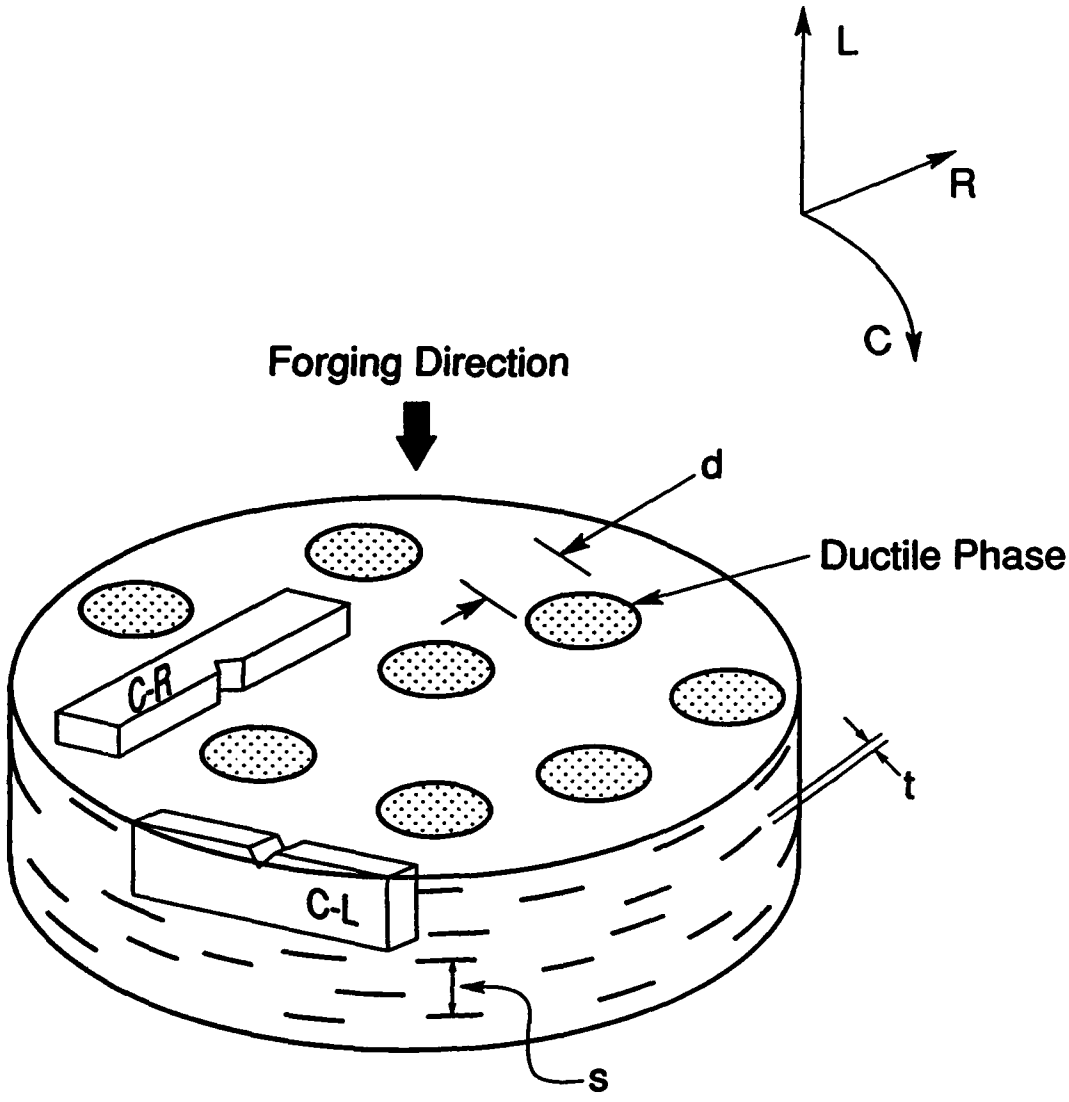

Fig. 2.2: Nomenclature for specimen orientations in cylindrical sections. L is the forging direction; R and C, refer to the radial and circumferential directions, respectively (21).

parallel to the crack-growth direction, were examined optically and in the SEM; parallel profiles were taken at the specimen mid-thickness location.

2.3 Results and Discussion

Fracture-Toughness Behavior: Compared to monolithic γ-TiAl which has a crack initiation toughness of ~8 MPa$\sqrt{m}$, the onset of cracking in the TiNb-reinforced composite occurs at approximately 15 MPa$\sqrt{m}$ and increases with crack extension to above 30 MPa$\sqrt{m}$, as shown by the resistance curve for the face and edge orientations in Fig. 2.3. The difference in crack-initiation toughness between the matrix and composite is believed to be partly due to crack trapping and renucleation effects. Subsequent increase in toughness with crack extension (R-curve behavior) can be attributed principally to crack bridging by unbroken ligaments of the TiNb phase in the wake of the crack tip (Figs. 2.4a,b), producing bridging zones of up to about 4 mm in length; additional toughening results from crack deflection and branching (Figs. 2.4b,c) that occurs as a consequence of crack-particle interactions. A limited amount of secondary cracking was also observed along the matrix side of the reaction-layer interface. In the face orientation, cracks are observed to renucleate out of plane (Fig. 2.4b) at the backs of the particles, especially at local strain-concentration sites where shear bands intersect the reaction layer/matrix. Crack paths are also deflected in the edge orientation by the highly-localized strain concentration within the TiNb phase. Toughening from these components is the combined effect of branched cracks, mixed-mode stress-intensity factors and asymmetric (out of plane) loading contributions. Finally, the resistance curves shown in Fig. 2.3 are influenced by specimen size and geometry, since small-scale bridging conditions do not prevail.

For small-scale bridging, the magnitude of toughening can be evaluated simply by accounting for the reduction in the near-tip stress intensity, K_{tip}, due to the bridging stress distribution, $\sigma(x)$, acting along the unbroken TiNb ligaments [10]:

$$K_{tip} = K^{\infty} - C \int_0^{\ell} [\sigma(x)/\sqrt{x}]dx \qquad (2.3)$$

where K^{∞} is the nominal (far-field) stress intensity, ℓ is the bridging-zone length, x is the distance from the crack tip and C is a geometric constant. For a specified stress distribution, $\sigma(x)$, large effects of finite-specimen size (large-scale bridging) have been demonstrated based on this approach [23]. However, these calculations may not be satisfactory in relating shielding to a more fundamental property of the composite, namely the stress-displacement function, $\sigma(u)$, of the TiNb particle.

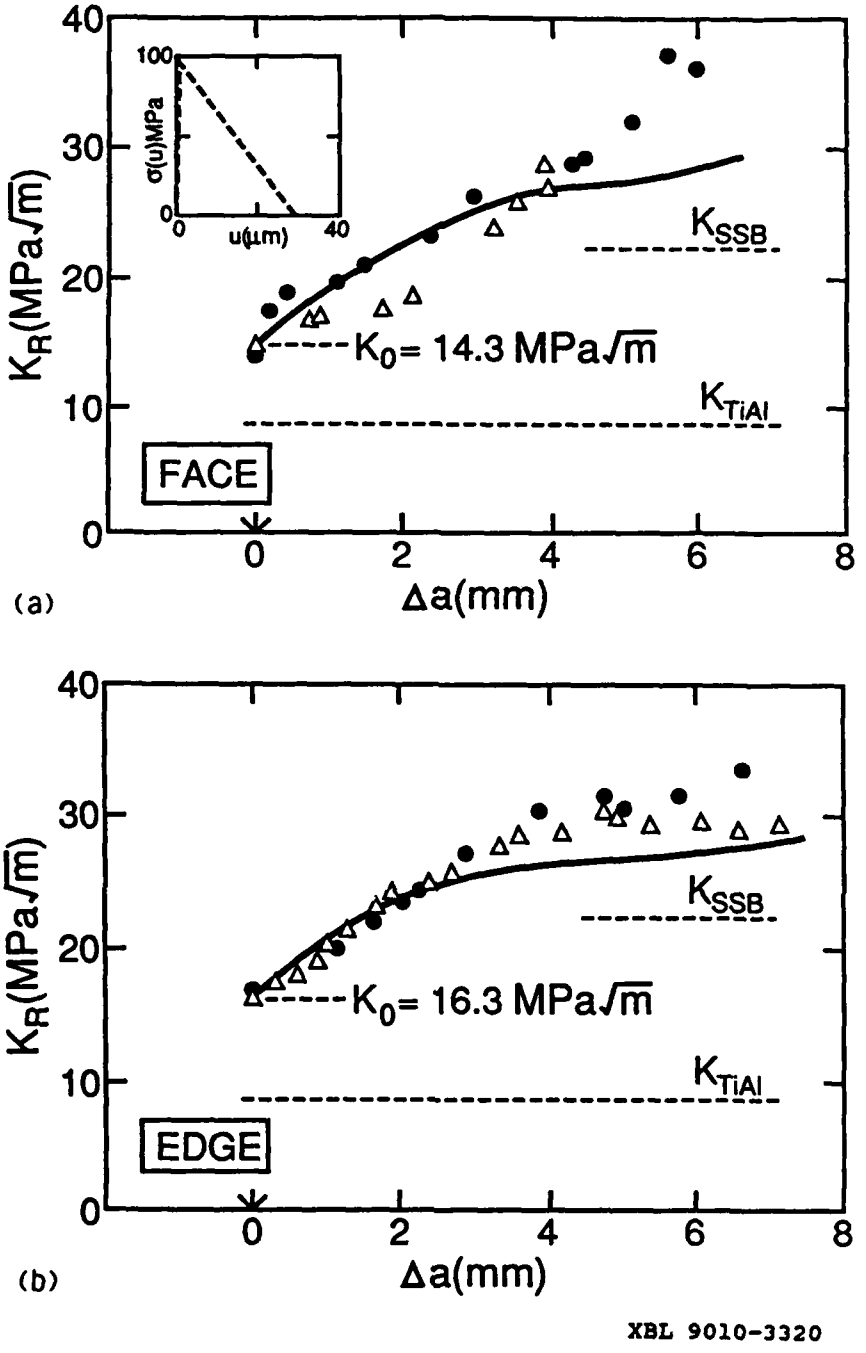

Fig. 2.3: R-curve behavior in γ-TiAl/TiNb intermetallic matrix composite in the (a) face (C-L) and (b) edge (C-R) orientations. The solid curves are calculated toughening increments from crack bridging, based on the stress-displacement function shown as an insert in Fig. 2.3a. Toughness of the γ-TiAl matrix (K_{TiAl}) and maximum steady-state toughness predicted by small-scale bridging calculations (K_{SSB}) are also plotted for comparison. The two sets of symbols represent crack-growth data on two different test specimens.

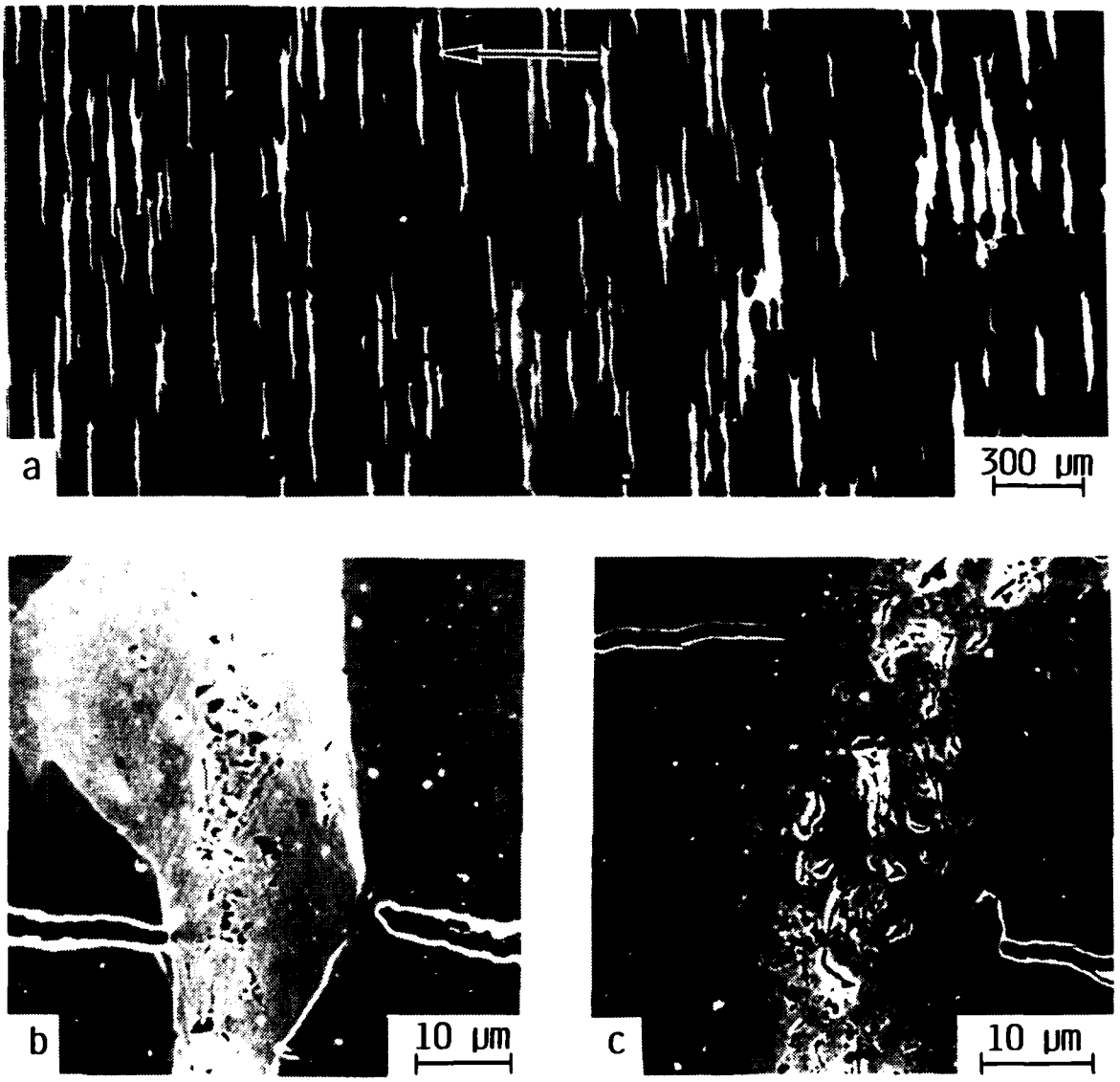

Fig. 2.4: (a) SEM micrographs of the in-plane crack-path morphologies (face orientation) in γ-TiAl/TiNb intermetallic composite under *monotonic loading*, showing evidence for (a,b) crack bridging by unbroken ligaments of ductile TiNb phase and (c) crack deflection and slight interfacial decohesion between the reaction layer and the matrix. Also note in (b,c) that the crack renucleates ahead of the TiNb particle in the TiAl matrix, when the crack intercepts the ductile phase. Arrow indicates the general direction of crack advance.

Alternatively, the bridging contribution to toughening for a given stress-displacement relationship can be described more accurately, under large-scale bridging conditions, by finding a *self-consistent* solution for the crack shape u(x), and stress distribution in the bridging zone $\sigma(x)$, for a specified $\sigma(u)$. These shielding calculations also require knowledge of the effective crack-tip toughness (K_o) and the plane-strain elastic modulus ($E' = E/(1-\nu^2)$, where ν is Poisson's ratio). A procedure for carrying out these calculations (see Appendix) has been developed [24], and the results are shown as solid lines in Fig. 2.3, for a $\sigma(u)$ function, measured using sandwiched-composite test specimens [11,12] and approximated in the form of a saw-tooth function (insert in Fig. 2.3a); the maximum stress was taken as $2.3f\ \sigma_y$ ($\approx$ 99 MPa) and the maximum opening displacement, u^*, as 0.6t (= 30 μm). The K_o was equated to the measured initiation toughness and E' was taken as 193 GPa.

The agreement between predicted and measured R-curves is generally quite good, particularly considering the idealizations inherent in the model [24] (e.g., continuous bridging vs. discrete, irregular and inhomogeneously distributed particles); deviations at larger crack extension are partly attributed to branching and deflection effects noted above. In addition, predicted differences between the quasi-steady state toughness and small-scale bridging values (shown by the dashed line in Fig. 2.3) are relatively modest. This behavior is due to the size and geometry dependence of the bridging-zone length as mediated by the crack shape u(x) to the shielding effect by particles with finite ductility; specifically, the larger effect of a given $\sigma(x)$ distribution in small test specimens is partially compensated for by the correspondingly smaller bridge lengths.

In summary, the significant toughening observed in the ductile-TiNb reinforced γ-TiAl composite can be understood by considering the contributions from crack trapping/renucleation, crack deflection/branching and crack-bridging mechanisms, as well as the effects of specimen size and geometry.

Fatigue-Crack Propagation: Corresponding crack-growth behavior in the γ-TiAl composite under cyclic loading conditions is shown in Fig. 2.5 in terms of the growth-rate per cycle as a function of the nominal stress-intensity range ΔK ($= K_{max} - K_{min}$); results for an unreinforced super-α_2-Ti_3Al (Ti-14Al-20Nb-3.2Mo-2V wt.%) intermetallic alloy are also shown for comparison. First, it is evident that under cyclic loads, cracks in the composite can propagate at stress-intensity levels below 6 MPa$\sqrt{m}$, far below that required to cause crack growth under monotonic loading on the R-curve. Second, in contrast to most metallic materials [25], yet similar to many ceramics [26], crack-growth rates in TiNb-TiAl have a marked power-law dependence on stress-intensity range; nearly five orders of magnitude variation in growth rates occur between ΔK levels of 5 and 7 MPa$\sqrt{m}$. In terms of the Paris power-law expression for

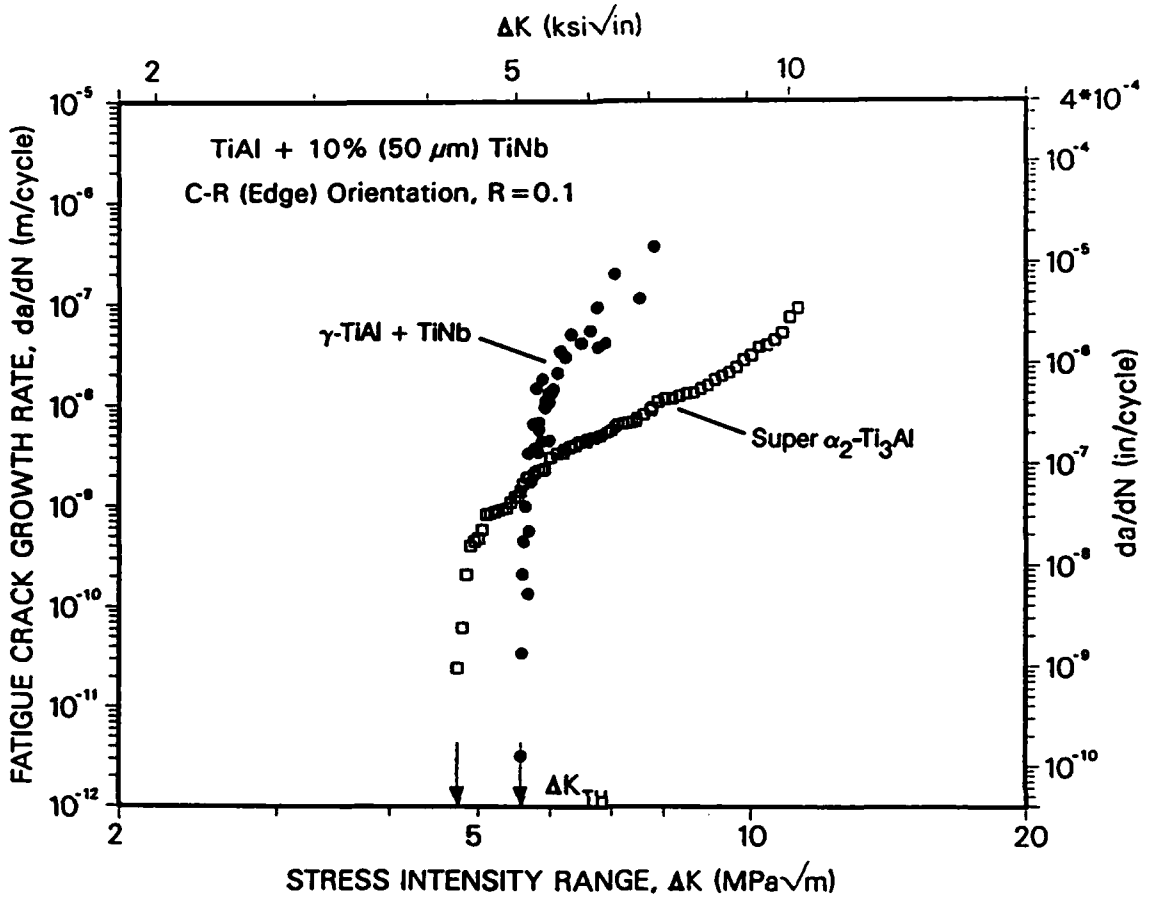

Fig. 2.5: Fatigue-crack propagation rates in TiNb-reinforced TiAl composite as a function of the nominal stress-intensity range, ΔK, at R = 0.1 (edge orientation). Growth-rate data on a monolithic super-α_2 Ti_3Al intermetallic alloy are also shown for comparison.

fatigue-crack propagation [27], specifically in the mid-growth rate regime; between 10^{-10} and 10^{-7} m/cycle, this gives a crack-growth relationship of:

$$da/dN = 2.2 \times 10^{-41} \Delta K^{42} \quad , \tag{2.4}$$

where da/dN is in m/cycle, and ΔK in MPa$\sqrt{m}$. By comparison, typical values of the exponent lie in the range 2 to 4 for metals [25] and ~20 to 50 for ceramics [22,26].

Scanning electron micrographs of the crack path and fracture-surface morphology for fatigue-crack growth in the composite are summarized in Figs. 2.6 and 2.7. In contrast to observations for monotonically loaded cracks (Fig. 2.4), there is no evidence of crack bridging, interfacial debonding or crack deflection in the plane of loading (Fig. 2.6a). In fact, metallographic sections of the fatigue cracks, taken across the specimen thickness at various distances behind the crack tip, show that all TiNb particles are cracked to within ~150 μm of the crack tip (Fig. 2.6b), *i.e., the large (up to 4 mm) bridging zones which are so prominent in enhancing the crack-growth toughness under monotonic loads completely diminish under cyclic loading*. The crack front can be seen to be continuous across the specimen thickness, with significant crack deflection and bifurcation *within* the ductile TiNb phase and no debonding or secondary cracking in the reaction product layers. Particle fracture under cyclic loading occurs by a transgranular-shear mechanism (Fig. 2.7), due to marked slip planarity in the TiNb phase; failure in the matrix, conversely, resembles transgranular cleavage with limited regions of intergranular failure (Fig. 2.7b).

Since the degree of crack bridging is small, the near tip and applied stress intensities are expected to be similar, except for shielding from other mechanisms such as surface roughness induced crack closure [28]. The small effect of bridging *per se* on the near-tip stress intensity in fatigue, however, could be estimated through periodic measurements of the bridging zone and the maximum and minimum crack opening displacements as a function of ΔK.

The cracking of the TiNb bridges is perhaps not too unexpected as metallic materials are known to be susceptible to fatigue; TiNb in particular has limited ductility and very low strain hardening and thus is especially prone to fatigue cracking. Moreover, since fatigue-crack advance can occur at stress-intensity levels as low as ~6-8 MPa$\sqrt{m}$, the toughening contribution from the deformation of unbroken bridges under cyclic loading would naturally be much smaller than that prevalent at the larger crack-opening displacements associated with monotonic crack-growth mechanisms at stress intensities in excess of ~20 MPa$\sqrt{m}$.

Such notions are consistent with other observations on the fatigue and fracture behavior of ductile/brittle material systems, e.g., metal/ceramic interfaces, in that fracture invariably predominates in the ceramic phase under monotonic loads due to its much lower toughness,

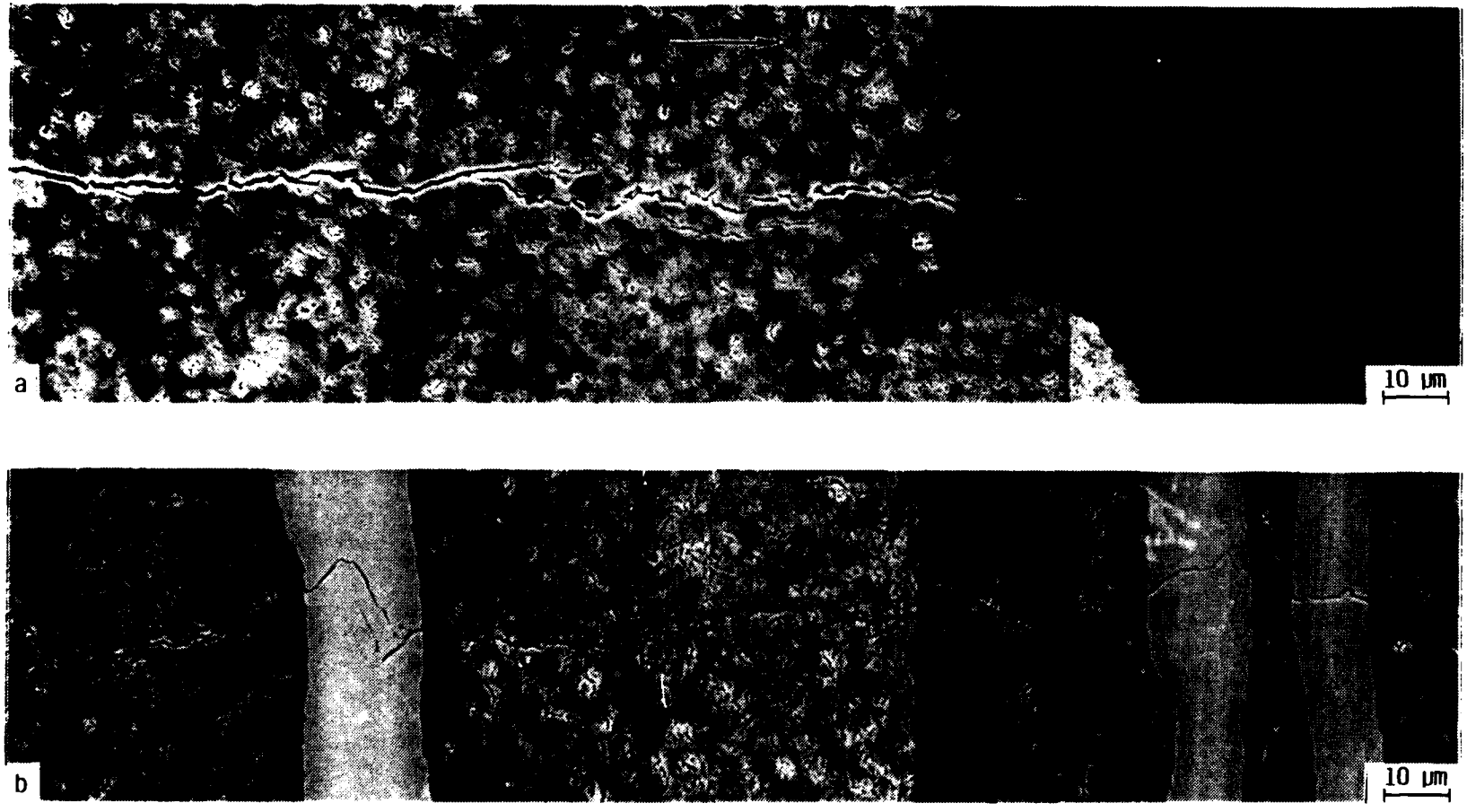

Fig. 2.6: SEM micrographs of crack-path morphologies in γ-TiAl/TiNb composite under *cyclic loading* (a) in the loading plane and (b) across the specimen thickness approximately 150 μm behind the crack tip (edge orientation). In contrast to Fig. 2.4, note that the crack propagates through ductile phase, showing no evidence of crack bridging by ductile particles during fatigue. Arrow indicates the general direction of crack advance.

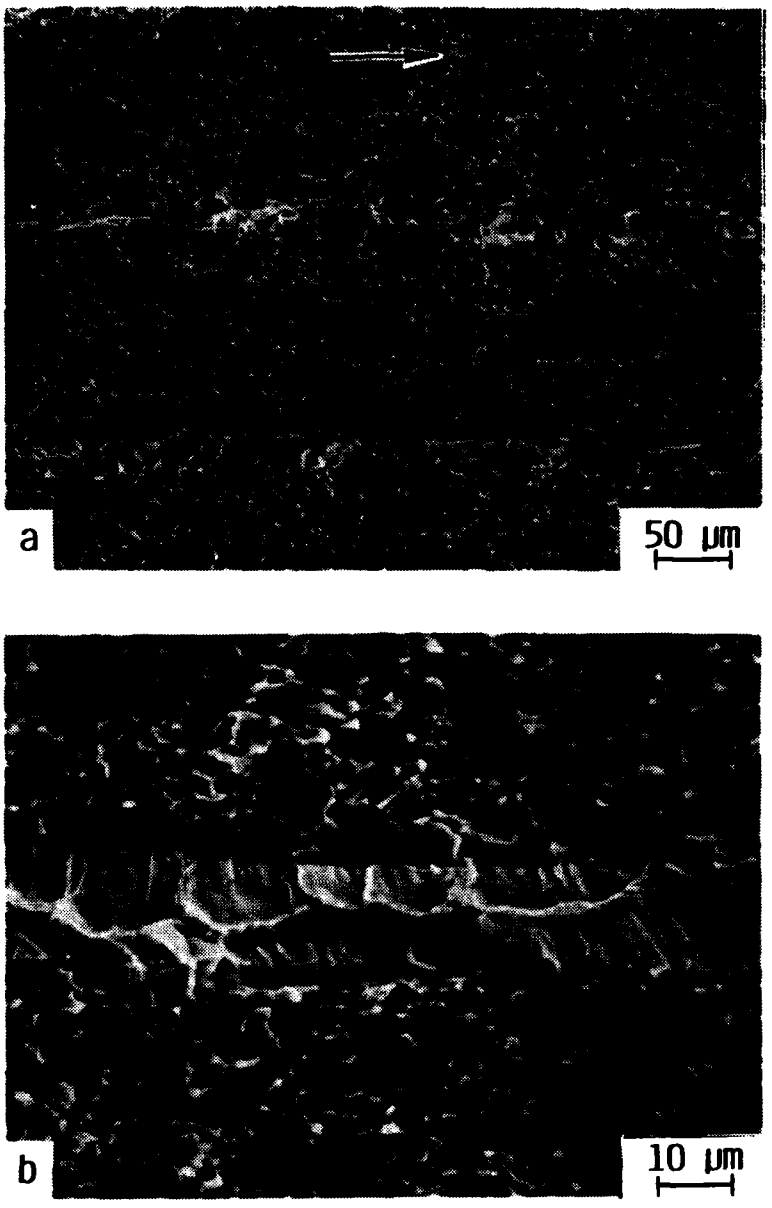

Fig. 2.7: (a) Low and (b) high magnification SEM micrographs of fatigue fracture surfaces in γ-TiAl/TiNb intermetallic composite. The TiNb particles fail by transgranular shear via localized planar-slip deformation while fracture in the matrix resembles transgranular cleavage. Note the absence of secondary interfacial cracking. Arrow indicates the general direction of crack growth.

whereas under cyclic loads the crack path reverts to the metal [29]. Recent crack-growth tests on (layered) aluminum-alloy/alumina compact-tension sandwich specimens, for example, clearly demonstrate near-interface cracking in the ceramic layer during R-curve testing, whereas in cyclic fatigue, cracks proceed in the metal layer, again close to the interface. The crack is presumably "attracted" to the metal phase under cyclic loads as the metal presents a region where strain can be accumulated to effect progressive crack advance; in essence, the metallic phase is simply more prone to fatigue failure.

The current results also demonstrate that composite microstructures developed for superior toughness may not necessarily result in optimum resistance to fatigue. In spite of the relatively strong TiNb/matrix interface in the present alloy, and low strain hardening of the metallic phase, crack bridging by high-strength TiNb particles significantly enhances toughness. However, the strong interface evidently provides little impedance to fatigue-crack growth under cyclic loading, which limits shielding from crack bridging. Apart from substituting ductile phases with better fatigue properties, the design of more fatigue-resistant, composite microstructures may very well involve weakened interfaces, where the resulting crack deflection and delamination at the particle/matrix boundary would delay cracking in the ductile phase, thereby promoting bridging at lower stress-intensity levels. Another viable approach may be to increase the connectivity of the ductile phase to promote crack meandering, thereby retarding fatigue-crack growth kinetics by enhanced crack-tip shielding from wedging of fracture-surface asperities (roughness-induced crack closure). Such concepts have been successful in the development of duplex ferritic/martensitic dual-phase steels with superior fatigue-crack growth properties [30]; they are now currently being evaluated in γ-TiAl/TiNb composites.

2.4. Conclusions

Based on a preliminary experimental study on the fracture toughness and cyclic fatigue-crack growth behavior in a γ-TiAl intermetallic alloy reinforced with 10 vol.% of $\sim$50 μm-thick ductile TiNb pancake particles, the following conclusions may be made:

(1) Under monotonic loading conditions, significant toughening of brittle γ-TiAl intermetallics can be achieved through the introduction of ductile TiNb particles. Mechanistically, the toughening results primarily from crack bridging by unbroken TiNb ligaments in the wake of the crack tip coupled with mechanisms associated with crack-particle interactions, i.e., crack trapping, renucleation and deflection. Compared to monolithic γ-TiAl which has a K_{Ic} fracture toughness of $\sim$8 MPa$\sqrt{m}$, the 10 vol.% TiNb-reinforced composite

shows improved crack-initiation toughness and significant R-curve behavior; steady-state toughness values exceed 25-30 MPa$\sqrt{m}$, with measured bridging zones approaching ~4 mm.

(2) Under cyclic fatigue loading, such ductile-particle toughening is found to be far less effective, due to the susceptibility of the ductile metallic phase to fatigue failure. As a result, there is no evidence of bridging by TiNb particles to within ~150 μm of the crack tip, and fatigue-crack propagation is observed at stress-intensity levels of ~6 MPa$\sqrt{m}$, far below those required to initiate cracking under monotonic loads.

2.5 References

1) R. L. Fleischer, D. M. Dimiduk and H. A. Lipsitt, *Ann. Rev. Mater. Sci.* **19**, 231 (1989).

2) R. L. Fleischer and A. I. Taub, *J. Metals* **41**:9, 8 (1989).

3) D. L. Anton, D. M. Shah, D. N. Duhl and A. F. Giamei, *ibid.*, 12 (1989).

4) P. J. Meschter and D. S. Schwartz, *J. Metals* **41**:11, 52 (1989).

5) Y. W. Kim, *J. Metals* **41**:7, 24 (1989).

6) E. L. Hall and S. C. Huang, *J. Mater. Res.* **4**, 595 (1989).

7) H. Dève and A. G. Evans, "Twin Toughening in Titanium Aluminide," in review.

8) T. Kawabata, M. Tadano and O. Izumi, *Scripta Metall.* **22**, 1725 (1988).

9) D. E. Larsen, M. L. Adams, S. L. Kampe, L. Christodoulou and J. D. Bryant, *Scripta Metall. Mater.* **24**, 851 (1990).

10) C. K. Elliott, G. R. Odette, G. E. Lucas and J. W. Sheckherd, in *High-Temperature/High-Performance Composites*, F. D. Lemkey, A. G. Evans, S. G. Fishman and J. R. Strife (eds.), MRS Symp. Proc., Vol. 120, 95 (1988).

11) H. E. Dève, A. G. Evans, G. R. Odette, R. Mehrabian, M. L. Emiliani and R. J. Hecht, *Acta metall. mater.* **38**, 1491 (1990).

12) G. R. Odette, H. E. Dève, C. K. Elliott, A. Harigowa and G. E. Lucas, in *Interfaces in Ceramic Metal Composites*, R. J. Arsenault, R. Y. Lin, G. P. Martins and S. G. Fishman (eds.), TMS-AIME, Warrendale, PA, 443 (1990).

13) M. F. Ashby, F. J. Blunt and M. Bannister, *Acta metall.* **37**, 1847 (1989).

14) H. C. Cao, B. J. Dalgleish, H. E. Dève, C. Elliott, A. G. Evans, R. Mehrabian and G. R. Odette, *Acta metall.* **37**, 2969 (1989).

15) B. D. Flinn, M. Rühle and A. G. Evans, *ibid.*, 3001 (1989).

16) V. V. Krstic and P. S. Nicholson, *J. Amer. Ceram. Soc.* **64**, 499 (1981).

17) P. Hing and G. W. Groves, *J. Mater. Sci.* 7, 427 (1972).

18) L. S. Sigl and H. E. Exner, *Metall. Trans. A* **18A**, 1299 (1986).

19) T. C. Lu, A. G. Evans, R. J. Hecht and R. Mehrabian, "Toughening of $MoSi_2$ with a Ductile (Niobium) Reinforcement," in review.

20) J. J. Lewandowski, D. Dimiduk, W. Kerr and M. G. Mendiratta, in *High-Temperature/High-Performance Composites*, F. D. Lemkey, A. G. Evans, S. G. Fishman and J. R. Strife (eds.), MRS Symp. Proc., Vol. 120, 103 (1988).

21) ASTM Standard E 399-83, *1989 Annual Book of ASTM Standards*, Vol. 3.01, ASTM, PA, 487 (1989).

22) R. H. Dauskardt and R. O. Ritchie, *Closed Loop* **17**:2, 7 (1989).

23) F. Zok and C. L. Hom, *Acta metall. mater.* **38**, 1895 (1990).

24) G. R. Odette and B. L. Chao, "A Large Scale Bridging Model for Ductile Phase Reinforced Composites," to be submitted to *Acta metall. mater.*.

25) R. O. Ritchie, *Int. Metals Rev.* **20**, 205 (1979).

26) R. H. Dauskardt, D. B. Marshall and R. O. Ritchie, *J. Amer. Ceram. Soc.* **73**, 893 (1990).

27) P. C. Paris and F. Erdogan, *J. Basic Eng., Trans. ASME* **85**, 528 (1963).

28) S. Suresh and R. O. Ritchie, *Metall. Trans. A* **13A**, 1627 (1982).

29) R. M. Cannon, B. J. Dalgleish, R. H. Dauskardt, T. S. Oh and R. O. Ritchie, *Acta metall. mater.* **39** (1991), in press.

30) J. K. Shang, J. L. Tzou and R. O. Ritchie, *Metall. Trans. A* **18A**, 1613 (1987).

31) A. G. Evans and R. M. McMeeking, *Acta metall.* **34**, 2435 (1986).

32) H. Tada, P. C. Paris and G. R. Irwin, *The Stress Analysis of Cracks Handbook*, Del Research Corp., St. Louis, MO (1985).

2.6 Appendix

Toughening Model: In cases where the size of the bridging zone is small compared to both the crack length and specimen dimensions, the effective toughness saturates at a steady-state level K_{SSB} corresponding to the steady-state bridge length (31). Under such small-scale bridging conditions, the steady-state toughening is mediated by the (plane strain) elastic modulus, E', the critical crack tip stress intensity required for crack extension, K_o, and the work-of-rupture of the reinforcements, ΔG_c (ca - Eqs. 1 and 2) as:

$$K_{SSB} = \sqrt{K_o^2 + E' \Delta G_c} \ . \qquad \text{(A2.1)}$$

In practice, however, small-scale bridging conditions are seldom encountered and it is necessary to model the effects of finite size and specific geometry (large-scale bridging) on toughening due to crack bridging including the rising portion of the resistance curve.

Rigorous modeling of large-scale bridging mechanics is carried out by calculating self-consistent solutions for the crack opening profile u(x), the crack-face stress distribution $\sigma(x)$, where x is the distance from the crack tip, for a specified set of "composite properties" including the stress-displacement relationship $\sigma(u)$, E', K_o and specified specimen geometry using an approach developed by Odette and Chao (24). The procedure is outlined as follows (Figure 2.A1):

1. A trial function, $\sigma(x)$, is used to calculate: (a) a trial reduction in crack-tip stress intensity (shielding) $\Delta K_b'$ from the bridging zone; and (b) the corresponding trial crack-face closure displacements $u_b'(x)$ by applying Castigliano's theorem. The requisite point-load stress intensity functions (in this case for the single-edge cracked specimen) are taken from Tada *et al.* (32). The resulting integrals are evaluated numerically, except for distances very near the crack tip where an analytical asymptotic solution is used.

2. The total trial applied stress intensity is taken as $K_p'(da) = K_o + \Delta K_b'$. A numerical integration, again based on Castigliano's theorem, is used to compute the trial crack-opening displacements $u_p'(x)$ due to the trial three-point bending load (P') corresponding to $K_p'(da)$.

3. A net trial crack opening is computed as $u'(x) = u_p'(x) - u_b'(x)$ and used to compute a trial $\sigma'(u)$ from the trial $\sigma'(x)$ and $u'(x)$.

4. The difference between the specified and trial stress-displacement functions is evaluated as $\varepsilon(u) = \sigma(u) - \sigma'(u)$, and the solution is achieved when $\varepsilon(u)$ is less than a specified convergence criterion.

5. If convergence is not achieved, the trial $\sigma'(x)$ is recomputed based on the trial $u'(x)$ and the specified $\sigma(u)$ and the process repeated starting at Step 1 above until convergence is achieved, usually in a few iterations.

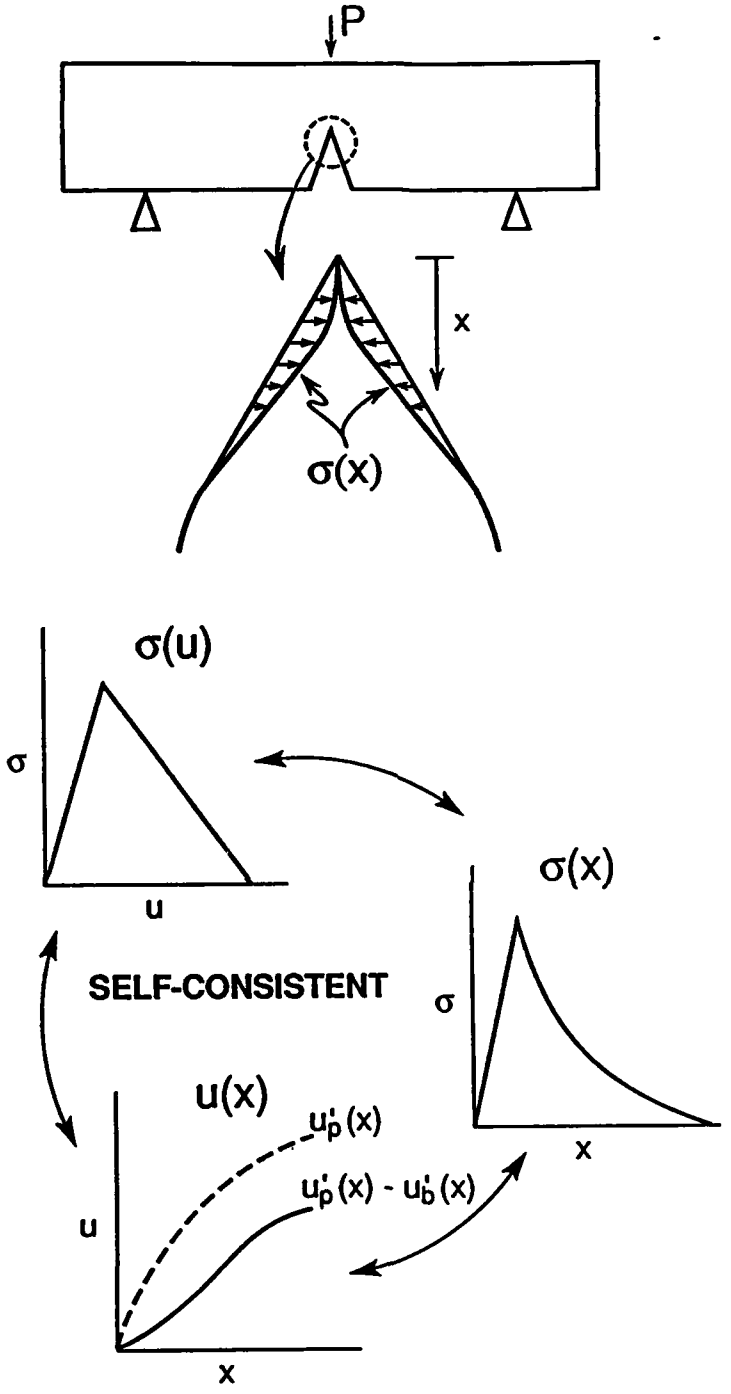

Fig. 2.A1:Schematic of the large scale bridging model computation applied to the three point bending geometry used in the experiments.

3. FABRICATION OF Nb_3Al INTERMETALLIC MICROSTRUCTURES

3.1 Introduction

Ductile-phase toughening concepts are currently being explored for the design and development of structural intermetallic alloys for advanced high-temperature applications in aerospace propulsion systems [1]. The notions are based on the simple fact that brittle cracking in the intermetallic can be impeded through the introduction of a tough, ductile phase that bridges the crack. Though the approach has proved to be effective under monotonic loading, very little is known about the fatigue resistance of such dual-phase (ductile-brittle) microstructures. It is therefore the objective of the present work to study the cyclic crack growth resistance of ductile-phase toughened microstructures, taking Nb_3Al/Nb as the model system. The advantage of the Nb_3Al/Nb system is that a wide variety of microstructures can be obtained by variation in composition and heat treatment. In addition, the processing can be performed *in house*, which allows the integration of results obtained to readily modify and develop better fatigue-resistant microstructures.

Such ductile-phase toughened microstructures are of particular interest for improving resistance to fatigue-crack propagation. Previous studies on dual-phase steels and α/β titanium alloys have shown that by developing duplex microstructures of hard and soft (ductile) phases, extensive crack meandering can be induced under cyclic loading, either by the crack deflecting at the hard phase or by following a continuous ductile phase [2,3]. Such crack-path morphologies are a potent source of crack-tip shielding, both from crack deflection and more importantly from fracture-surface asperity-induced crack wedging (roughness-induced crack closure); in fact, the highest fatigue-crack growth threshold ever measured at ambient temperatures in a metallic material has been achieved with this technique [4]. Accordingly, the development of such novel microstructures, for example to induce such crack meandering, will be attempted to optimize fatigue performance.

3.2 Background

Niobium metal of sufficient purity is tough, ductile and exhibits a unique combination of mechanical and physical properties. It is the lightest of the refractory metals, with a density close to that of copper (7.29 g/cm^3), and has good thermal conductivity for heat transfer applications. Although niobium retains a useful degree of strength above 1000°C, it oxidizes very rapidly, in pure or unprotected oxygen-bearing environments at these temperatures. However, there are a number of alloys of niobium and aluminium, with other alloying additions that effectively improve the oxidation resistance. One such system, is based on the intermetallic

alloy, Nb_3Al, which meets the requirements as an useful high-temperature structural material [5,6]. This alloy is preferred over Nb_2Al and $NbAl_3$ intermetallics due to its higher melting temperature (1960°C), as seen from the Nb-Al binary phase diagram in Fig. 3.1.

However, like many intermetallics that exhibit high melting points and high elastic moduli, Nb_3Al also has a low-symmetry, complex crystal structure (A-15). Although this structure is responsible for its high-temperature strength, it concurrently limits the number of slip systems, increases the slip vector, restricts cross slip and transfer of slip across grain boundaries [7,8], all factors which intrinsically contribute to its limited ductility, fracture toughness and tendency for brittle fracture at ambient temperatures. Accordingly, currently Nb_3Al has limited structural use, despite its promising properties at elevated temperatures.

One of the approaches to improving the ductility and toughness of a brittle intermetallic is to fabricate a composite by incorporating a ductile phase so as to impede crack advance by ductile-ligament bridging [9]. This may be accomplished either by artificially hybridizing the microstructure through powder-metallurgy techniques or *in-situ* precipitation reactions based on phase transformations in the alloy system. In the case of binary Nb-Al, the peritectic reaction at 1960°C (Fig. 3.1), involving the precipitation of Nb_3Al from the liquid and high-temperature Nb solid solution (Nb_{ss}), can be utilized for fabricating two-phase microstructures of Nb_{ss} in a brittle Nb_3Al matrix [10], viz:

$$\text{Liquid} + Nb_{ss} \longrightarrow Nb_3Al$$

Previous studies have shown this to be a sluggish transformation, such that the Nb solid solution can be fully retained at room temperature with only a moderate degree of undercooling [11-13]. Subsequent heat-treatment precipitates the ordered Nb_3Al phase. The precipitation reaction is shown to be a massive transformation resulting in a highly uniform and fine distribution of a filamentary niobium within a non-continuous Nb_3Al matrix. Such a duplex Nb/Nb_3Al microstructure can potentially enhance toughness and crack-growth resistance by crack bridging, with an additional contribution from the deformation of the ductile phase in the latter case.

Vacuum hot pressing and reactive sintering are two techniques that are widely used for powder processing of materials. Compared to arc melting and casting, powder processing offers the advantage of controlling the cooling rate since resistance heating is employed. In addition, since hot-pressing operations are conducted in a closed or semi-closed system of cans and dies, volatization is minimized, and densification is accomplished at temperatures substantially below the melting point of the intermetallic compound. Accordingly, both vacuum hot pressing and reaction sintering techniques have been used to fabricate dual-phase Nb_3Al/Nb microstructures.

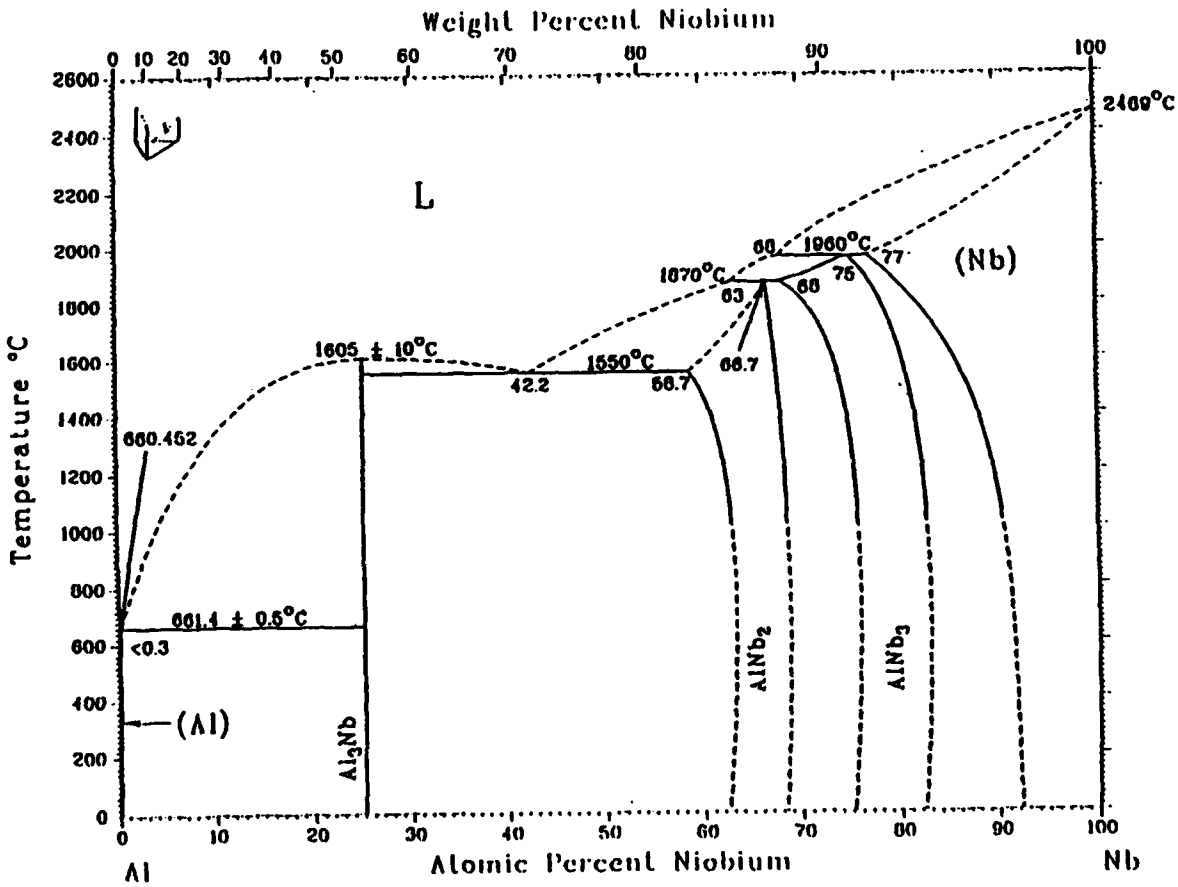

Fig. 3.1: The Nb-Al binary phase diagram [11].

A preliminary assessment of the extent of toughening in these microstructures has been obtained using indentation techniques.

3.3 Materials and Experimental Procedures

Preparation and synthesis of powders: Commercially pure niobium powder was obtained from Cerac Inc., Milwaukee, WI. As the niobium powder available commercially was fairly coarse (~8 μm), as shown in Fig. 3.2a, it was necessary to grind it to a size of ~1 μm, roughly a third of the size of Al powder (~3 μm). Since niobium powder is ductile and cannot be effectively ground in a ball mill, it was converted into brittle $NbH_{0.89}$. This involved hydrogenation of the Nb powder in an alumina boat, kept in a furnace under 100% hydrogen gas atmosphere, at 700-750°C for 20 minutes. The furnace was then cooled at 3°C/minute with the hydrogen gas being constantly recharged to maintain a pressure of 1-1.5 atmospheres [14]. The hydrogenated powder was subsequently ground using WC-Co balls in a ball mill for 12-16 hours under hexane liquid, to prevent oxidation. When the powder size was about 1-2 μm, it was dehydrogenated by heating to 1200°C under vacuum and holding for 30 minutes. Scanning electron micrographs of the fine ground Nb powder and atomized aluminum powder (obtained from Valimet Inc., Stockton, CA) are shown in Figs. 3.2b and 3.2c, respectively.

The powders were mixed in the ratio of Nb-7wt.% Al (Nb-20.6at.% Al) and the mixture was ball milled for 2 hours. Synthesis of the mixed powders was carried out by heating in vacuum to 1200°C at a rate of 20°C/minute, held at this temperature for an hour and stored under argon to prevent oxidation. As shown in Fig. 3.3, the reaction between the powders is only partly complete at this stage leaving regions of pure Al and Nb in the compact.

Vacuum Hot-Pressing: A 38 mm diameter graphite die was used to hold the synthesized powder and hot pressing. Several samples were fabricated in a single operation by separating the powders by graphite discs, coated with a boron nitride lubricant to prevent welding between graphite and the Nb-Al powder. The compacted powders were then hot-pressed by simultaneously increasing the pressure and temperature to 36.2 MPa (5.4 ksi) and 1650°C, respectively, maintained at these values for 10 minutes, and cooled to room temperature (Fig. 3.4). The final samples were obtained as disks, ~38 mm in diameter and ~4 mm thick, from hot pressing ~40 gms of synthesized Nb and Al powder.

Reaction Sintering: The synthesized Nb-Al powder was cold compacted at 365 MPa (55 ksi) pressure, and reaction sintered by heating the synthesized powder to 1200°C in a helium atmosphere and holding at this temperature for an hour, to initiate the reaction:

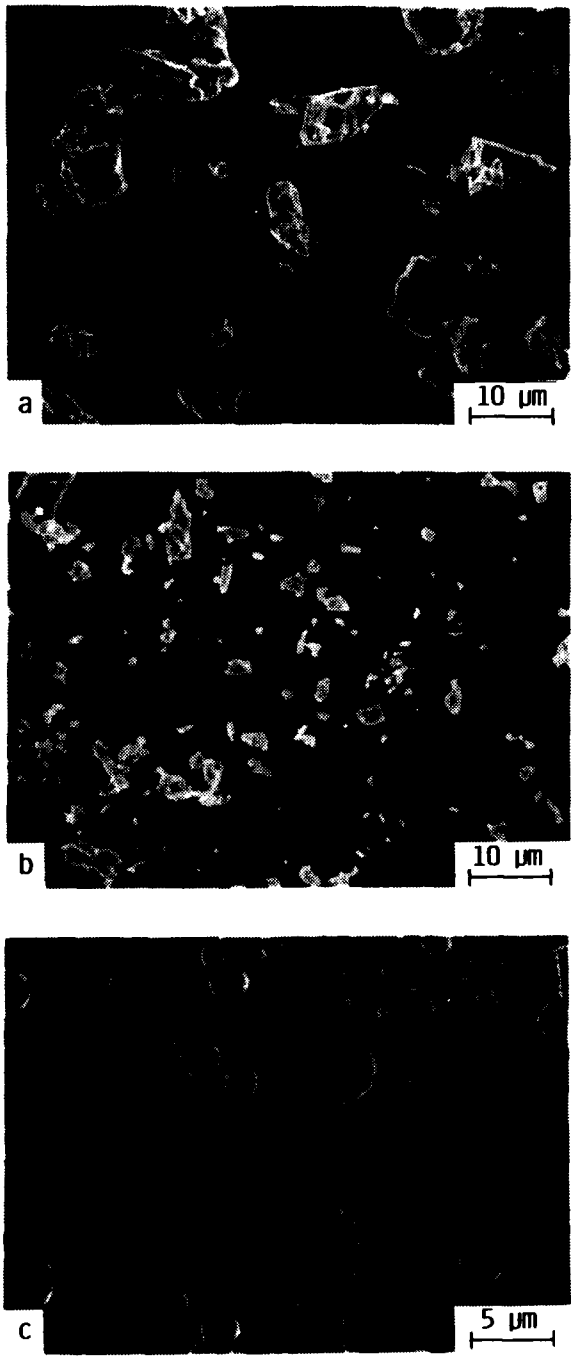

Fig. 3.2: SEM micrographs of (a) coarse, commercial-grade Nb powder, (b) fine Nb powder after hydrogenation, grinding and dehydrogenation and (c) commercial Al powder.

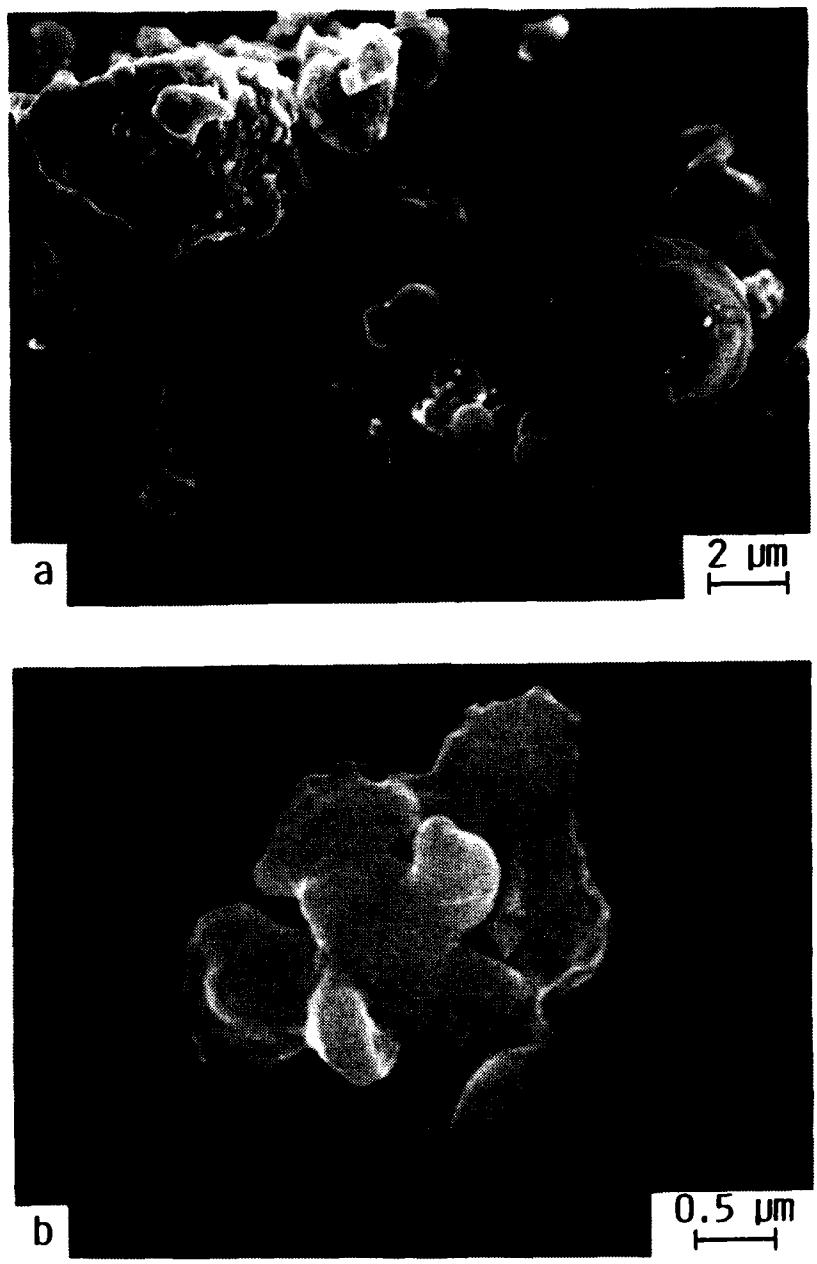

Fig. 3.3: Synthesized Nb-Al composite powder showing (a) regions of Nb and Al segregation and (b) the formation of Nb_3Al.

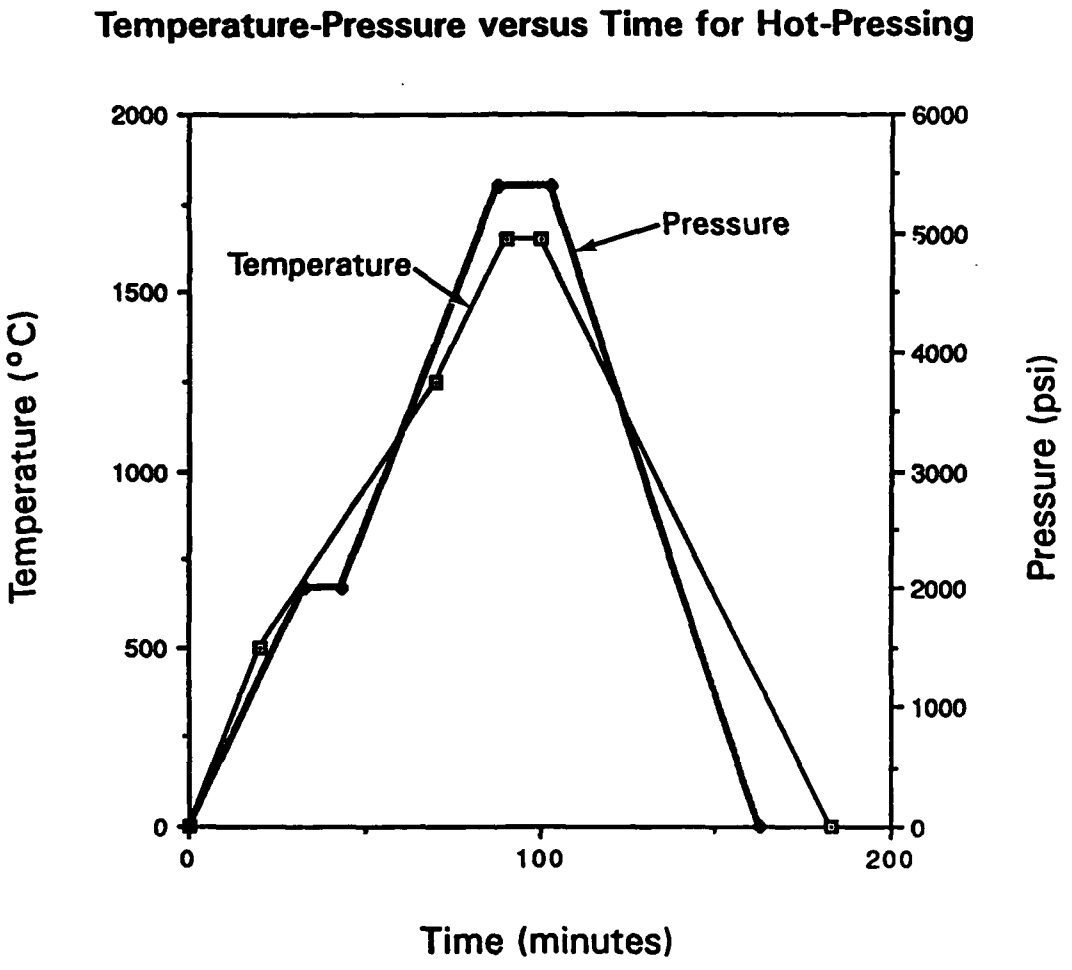

Fig. 3.4: Temperature and pressure schedules used during hot pressing.

$$3\,Nb + Al \longrightarrow Nb_3Al$$

Since the reaction is exothermic, it is expected that densification of the powders can be readily achieved at this temperature. Degassing was performed by holding the compacts at 500°C for 10 hours prior to attaining the reactive-sintering temperature. Samples were subsequently furnace cooled to room temperature.

Thermal Treatment: To examine the nature of phase transformations and the sequence of microstructural development, both the hot-pressed and reaction-sintered samples were then heat treated in vacuum at 1800°C for 1, 4, and 24 hours, and furnace cooled to room temperature.

Metallography and Toughness Testing: Sections of all samples were mounted and metallographically polished using 220, 600 and 1200 grit SiC paper, and then 6 and 1 μm diamond paste; final polishing was accomplished using mastermet slurry. Samples were etched using a solution of 10 ml HNO_3, 10 ml HF and 30 ml lactic acid to reveal the microstructural features and examined on the optical and scanning electron microscopes. X-ray diffraction (XRD) analysis was performed on all samples to identify the various phases present in the different microstructures.

Measurement of fracture toughness K_{Ic} was performed using indentation techniques. Polished samples were indented with a Vickers diamond indentor at loads of 10.0 and 14.5 kg to initiate cracking. In addition, Rockwell R_c hardness values were obtained for all the samples.

3.4 Results and Discussion

Primary Microstructures: Fig. 3.5 shows the scanning electron micrograph (SEM) of the microstructure obtained upon hot-pressing the synthesized Nb-7wt.% Al powders at 1650°C, and the corresponding XRD pattern. As expected from the phase diagram (Fig. 3.1), a dual-phase microstructure of a Nb_3Al matrix with niobium solid solution dispersed as the second phase is obtained. Energy dispersive X-ray spectroscopy (EDS) analysis confirmed the matrix to be Nb-23at.% Al (Nb_3Al) and the second phase to be Nb_{ss} with 12.5at.% Al. The corresponding XRD pattern also shows peaks characteristic of Nb_3Al and Nb. The Nb_3Al peaks are slightly displaced to the left of actual stoichiometry (Nb-25 at.% Al), while the Nb peaks are displaced to the right of the peaks expected for pure Nb. This indicates that Nb is in the form of a solid solution with a slightly decreased lattice parameter ($a_{Nb_{ss}}$ = 0.3275 nm, a_{Nb} = 0.3305 nm), accounting for the peak shift towards higher 2Θ values [11]. Similarly the Nb_3Al obtained has a slightly higher lattice parameter than stochiometry. In the as hot-pressed

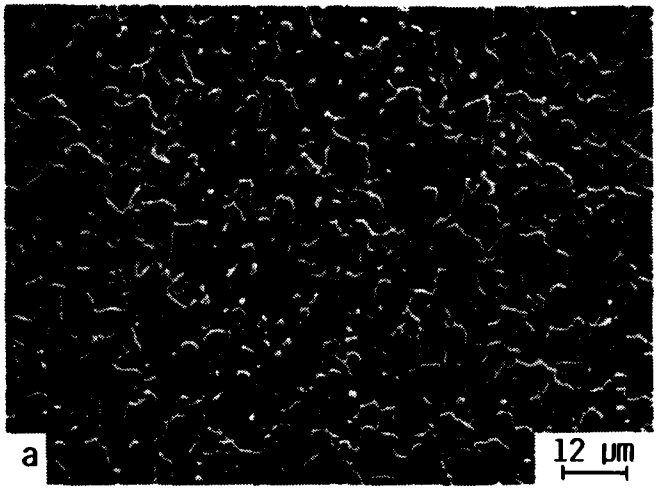

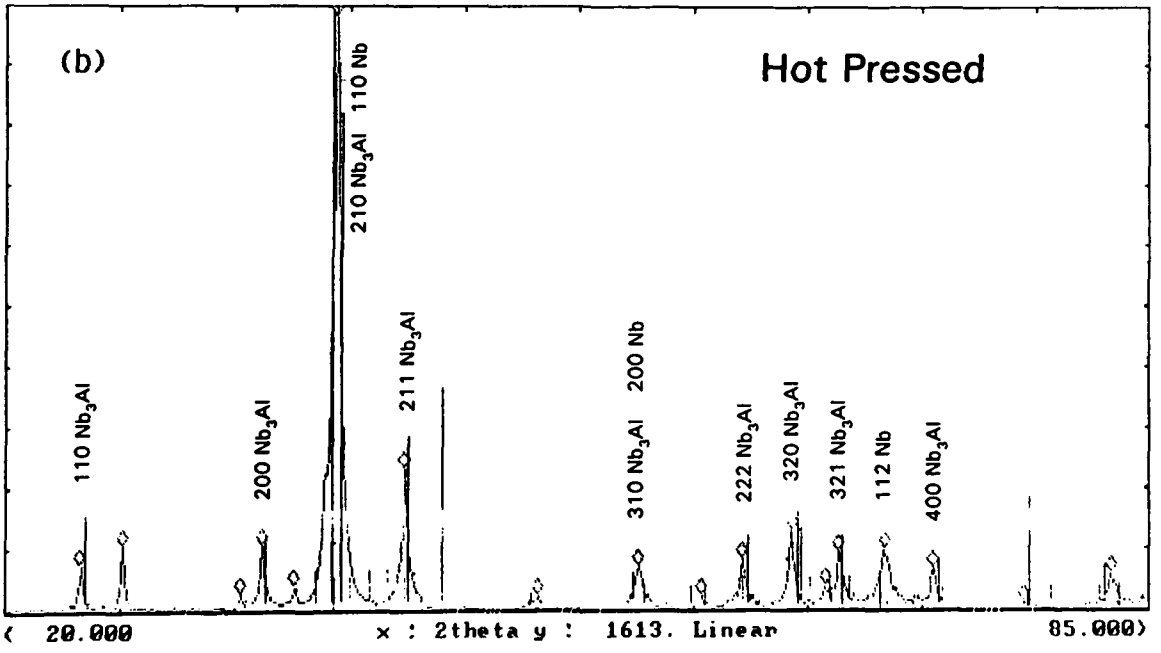

Fig. 3.5: (a) Microstructural features of the as hot-pressed Nb-7wt.% Al sample showing Nb_3Al matrix with islands of Nb (solid solution) phase, and (b) corresponding XRD pattern showing characteristic peaks of Nb_3Al and Nb.

condition, the microstructure exhibited a R_c hardness of 56.0±1.0 and an indentation toughness (10 kg load) of K_{Ic}=6.5±1.2 MPa$\sqrt{m}$.

Corresponding microstructures and XRD patterns for reaction-sintered samples are shown Fig. 3.6. The structure appears relatively porous, compared to the hot-pressed condition, suggesting that the reaction between the Nb and Al powders has not been completed, thereby resulting in a lower degree of densification. Hardness and toughness values were difficult to measure due to sample break-up during load application. Features on the X-ray diffraction pattern are more or less similar to the hot-pressed sample, showing characteristic peaks of Nb_3Al and Nb.

Influence of Thermal Treatment: Fig. 3.7 illustrates the different microstructures obtained upon heat treating the as hot-pressed and reaction-sintered Nb-7wt.% Al alloys for 1, 4 and 24 hours at 1800°C; details of the X-ray intensities are summarized in Fig. 3.8. In the hot-pressed sample, aging for an hour results predominantly in a matrix rich in niobium (Nb-7at.% Al) with micron-sized Al-rich particles and a small volume fraction of the Nb_3Al phase (Fig. 3.7a). Following aging for four hours, the amount of Nb_3Al decreases; the microstructure consists of Nb_{ss} matrix with particles rich in Al (Fig. 3.7b). Very fine substructural features are also evident in the matrix, and become more prominent with increased aging time (Figs. 3.7b,c), associated with the decomposition of Nb_{ss} according to the peritectic reaction. On aging for 24 hours at 1800°C the transformation appears to be nearly complete; both primary and secondary Nb_3Al dendrite arms are fully developed within the grains, and the microstructure now features lamellar Nb_3Al with a "stringy" second phase of the Nb solid solution. The Nb_{ss} phase is rather fine, on the order of a few microns thick and very uniformly distributed throughout the matrix. Nominally similar microstructural features may be noted for reactive-sintered samples (Figs. 3.8d-f).

The formation of primary and secondary dendrites of Nb_3Al, later in the aging sequence is believed to be due to the sluggish nature of the phase transformation which may be achieved at temperatures as low as 1000°C [11]. The width and distribution of the niobium phase is dependent on the temperature at which this massive transformation occurs. In fact, transmission electron microscopy studies by Marieb and Nutt [15] on Nb_3Al-based alloys processed at 1200°C show microstructures with highly dislocated filaments of niobium interspaced between thick plates of ordered Nb_3Al.

Variations in hardness and indentation toughness are consistent with the sequence of phase transformation. Results are summarized in Fig. 3.9, where the indentations (at 14.5 kg) on the various hot-pressed Nb-7wt.% Al microstructures are shown. Compared to the as hot-pressed structure which has an initial R_c hardness of ~56, the hardness decreases to values of

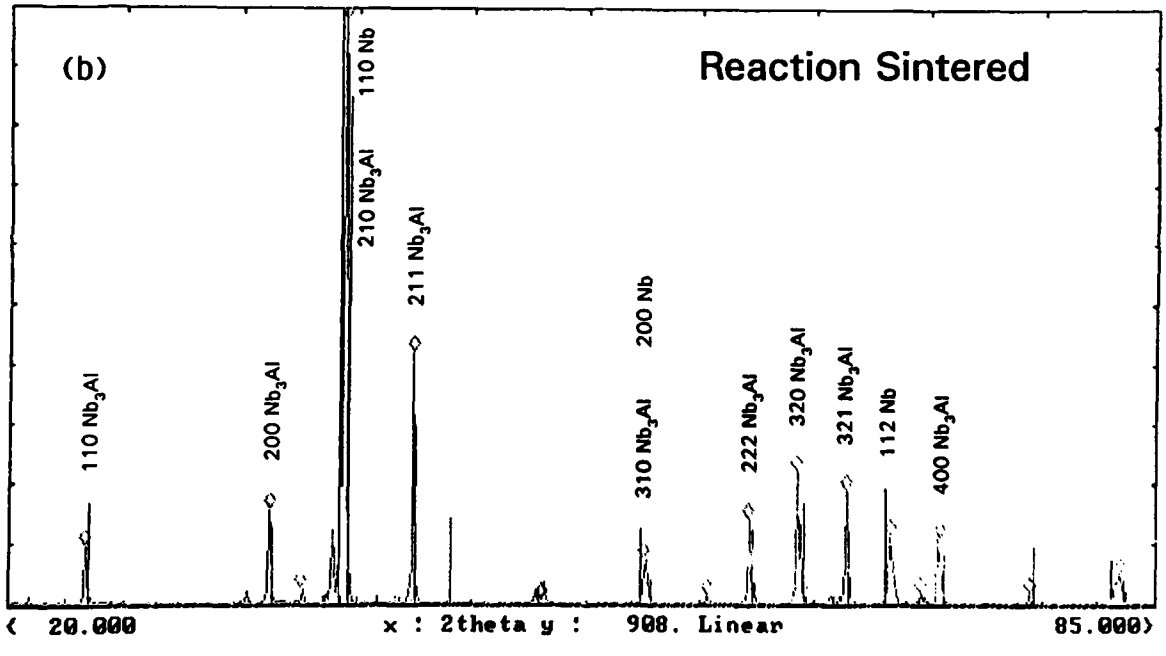

Fig. 3.6: (a) Microstructural features of the as reaction-sintered Nb-7wt.% Al sample showing a highly porous structure, without any clear features, and (b) corresponding XRD pattern indicating the characteristic peaks of Nb_3Al and Nb.

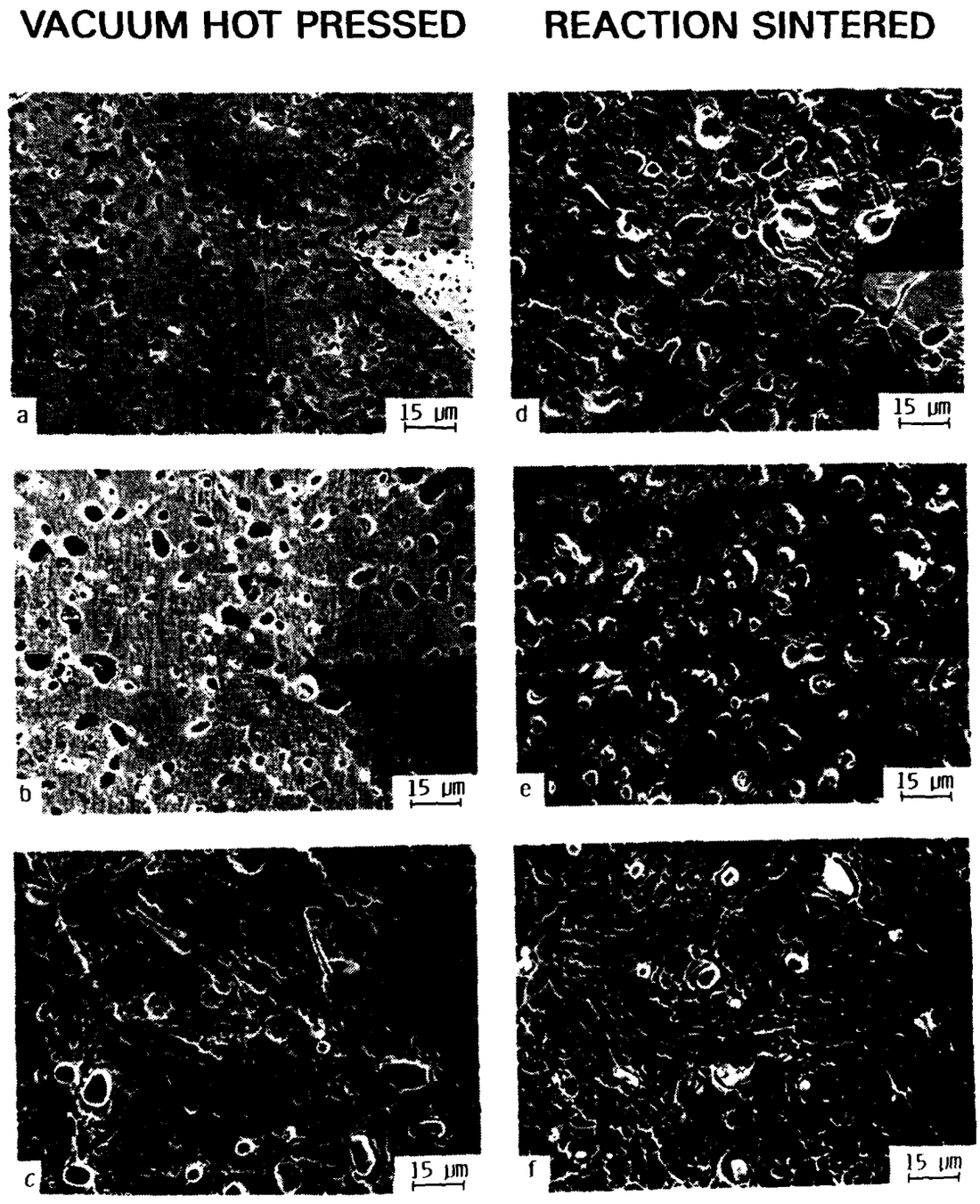

Fig. 3.7: (a)Variation in the microstructure for (a,b,c) hot pressed and (d,e,f) reaction sintered samples, following heat treatment at 1800°C for (a,d) 1 hr, (b,e) 4 hr and (c,f) 24 hr.

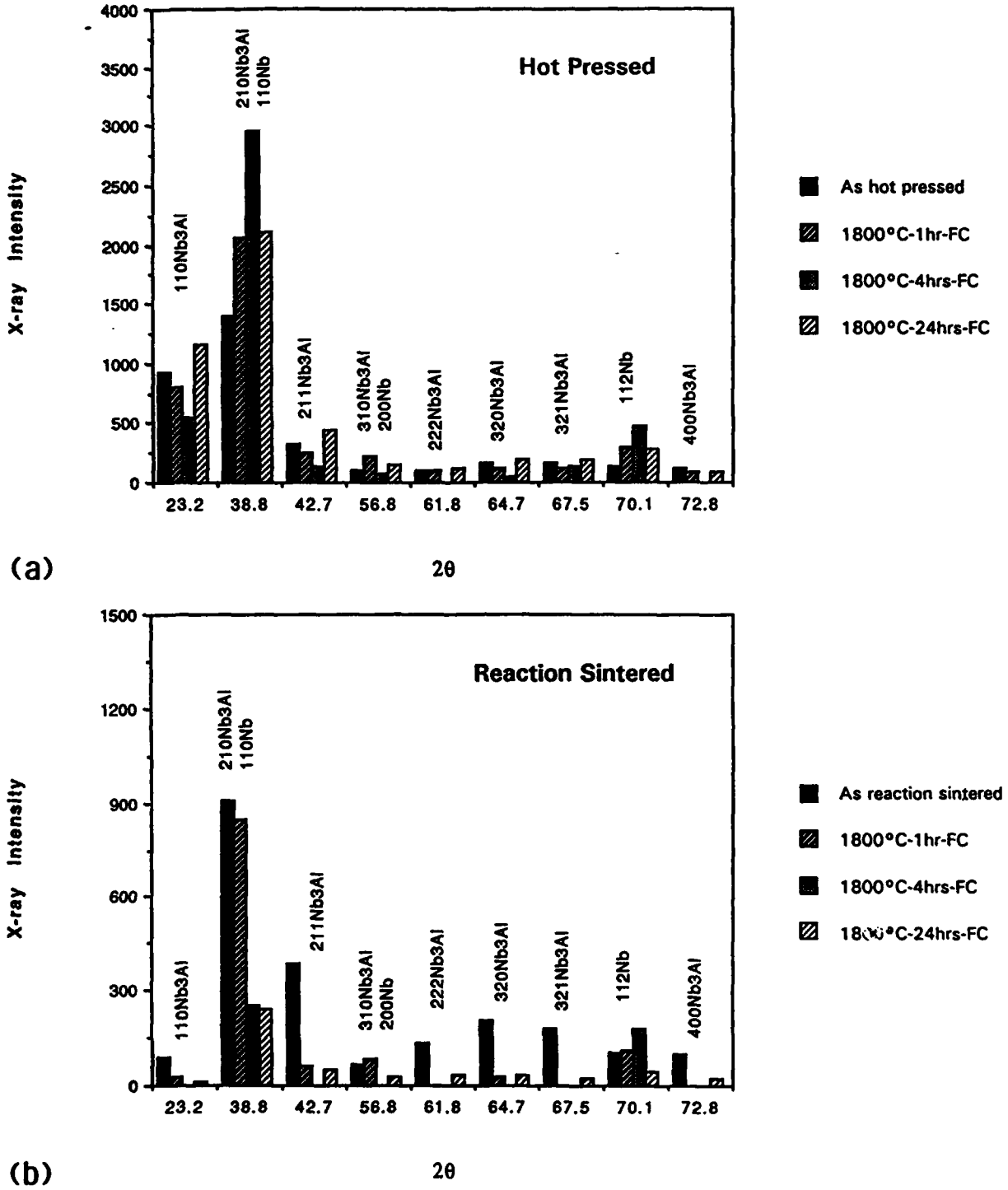

Fig. 3.8: Variation in X-ray peak intensities corresponding to Nb and Nb_3Al phases with thermal treatment for (a) hot-pressed and (b) reaction-sintered samples.

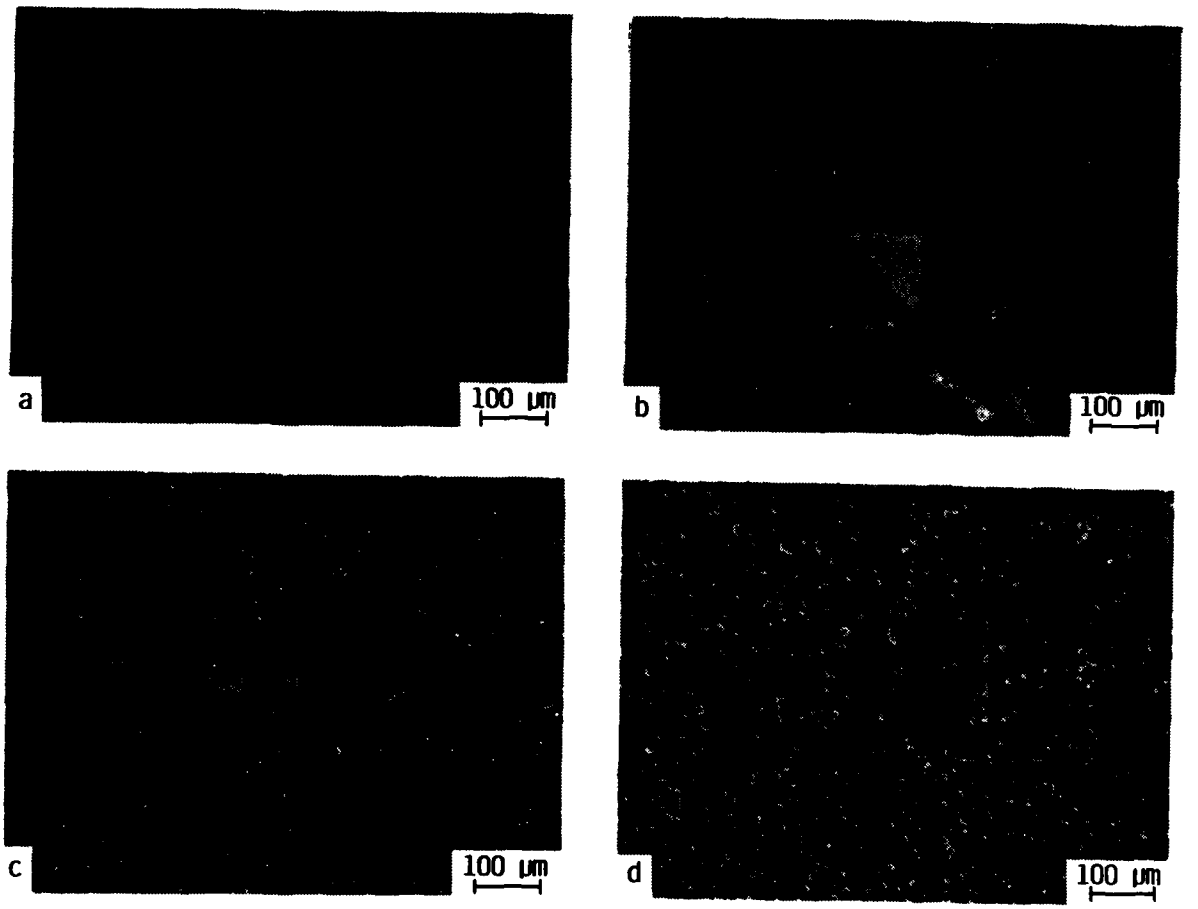

Fig. 3.9: SEM micrographs of Vickers-hardness indents obtained using a 14.5 kg load in microstructures fabricated by (a) hot-pressing, and following aging at 1800°C for (b) 1, (c) 4, and (d) 24 hours.

~37 and ~30, upon aging for 1 and 4 hours, respectively, as the volume fraction of Nb_3Al decreases and the microstructure contains predominantly Nb_{ss}. On prolonged aging for 24 hours, however, the hardness again increases to R_c ~55, concurrent with the decomposition of the Nb_3Al intermetallic. Similar results were seen for the alloy processed by reactive sintering; R_c hardness values were 42, 19 and 56 for microstructures obtained after aging at 1800°C for 1, 4 and 24 hours, respectively.

Estimated values for toughness of Nb-7wt.% Al alloy in the fully-developed dual-phase Nb_3Al/Nb microstructure, after thermal treatment for 24 hours at 1800°C, are $\sim 7.5 \pm 1.0$ MPa$\sqrt{m}$. The values are quite similar to those obtained in the as hot-pressed condition. In both these conditions, there is evidence of toughening from crack bridging by the ductile Nb_{ss} phase, present either as islands (Fig. 3.10a) or as fine filaments between interdendritic channels of Nb_3Al (Fig. 3.10b); cracking is apparent in the hard-Nb_3Al intermetallic phase with the Nb particles remaining intact. No cracks are observed for the intermediate Nb_{ss}-rich microstructures at the indendation loads (14.5 kg) applied; toughness values are expected to be in excess of ~10 MPa$\sqrt{m}$.

3.5 Conclusions

High temperature Nb_3Al intermetallic alloys reinforced with ductile Nb have been processed successfully using reactive sintering and vacuum hot-pressing techniques to generate model microstructures for the purpose of studying the resistance of duplex intermetallic/metal structures to cyclic fatigue damage. Utilizing the peritectic reaction in the phase diagram, a range of Nb/Nb_3Al microstructures has been obtained by thermal treatments. Specifically, a duplex microstructure of Nb_{ss}/Nb_3Al intermetallic alloy with a fine stringy Nb phase was achieved by treating a powder-processed Nb-7wt.% Al alloy at 1800°C for 24 hours. Preliminary indentation-toughness measurements indicate that the Nb phase contributes to toughening by bridging the cracks in the non-continuous Nb_3Al matrix; however, the role of such toughening under cyclic loading may be quite different and is currently under examination.

3.6 References

1) J. J. Stephens, *J. Metals* 42, 22 (1990).

2) V. B. Dutta, S. Suresh and R. O. Ritchie, *Metall. Trans. A* 15A, 1193 (1984).

3) J. M. Larsen, J. C. Williams and A. W. Thompson, in *Mechanics of Fatigue Crack Closure*, ASTM STP 982, J. C. Newman and W. Elber (eds.), ASTM, Philadelphia, PA, 149 (1988).

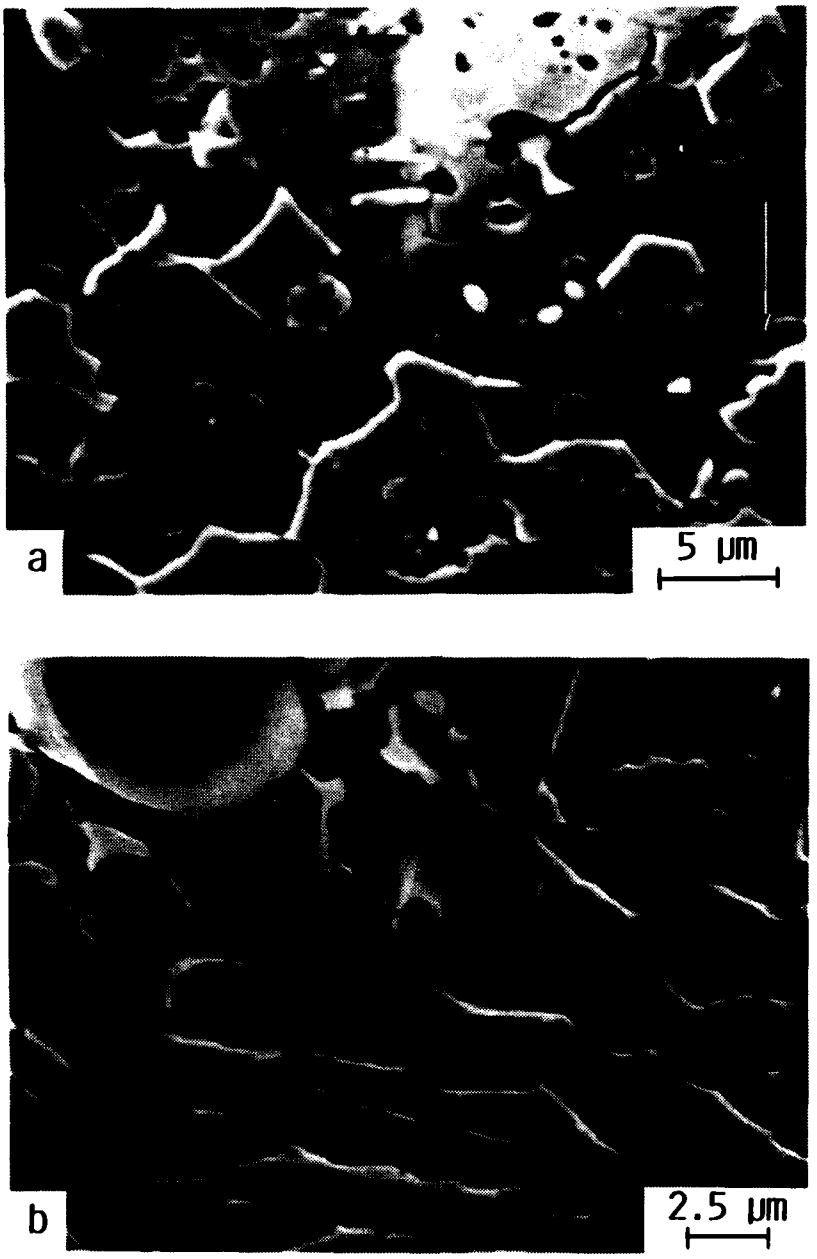

Fig. 3.10: High-magnification SEM micrographs of crack-path morphologies emanating from indents during indentation toughness tests in (a) as hot-pressed and (b) 24 hour heat-treated samples, showing crack bridging by the islands and filaments of Nb_{ss} phase. Arrow indicates direction of cracking.

4) J. K. Shang, J. L. Tzou and R. O. Ritchie, *Metall. Trans. A* **18A**, 1613 (1987).

5) D. L. Anton, D. M. Shah, D. N. Duhl and A. F. Giamei, *J. Metals* **41**, 12 (1989).

6) D. L. Anton and D. M. Shah, in *High Temperature Structural Intermetallic Compounds*, C. T. Liu et al. (eds.), MRS, Pittsburgh, PA (1989).

7) C. T. Liu and J. O. Stiegler, *Science* **226**, 636 (1984).

8) E. M. Schulson, *Int. J. Powder Met.* **23**, 25 (1987).

9) I. Baker and P. R. Munroe, *J. Metals* **40**, 28 (1988).

10) L. S. Sigl, P. A. Mataga, B. J. Dalgleish, R. M. McMeeking and A. G. Evans, *Acta Metall.* **36**, 945 (1988).

11) C. E. Lundin and A. S. Yamamoto, *Trans. Met. Soc. AIME.* **236**, 863 (1966).

12) L. Kohot, R. Horyn and N. Iliev, *J. Less Common Metals.* **44**, 215 (1976).

13) L. Jorda, R. Flukinger and J. Miller, *J. Less Common Metals* **75**, 227 (1980).

14) O. Kanou, M.S. Thesis, University of California, Berkeley (1990).

15) T. Marieb, M.S. Thesis, Brown University (1989).

4. BRIEF SUMMARY OF FUTURE WORK

4.1 TiAl and $MoSi_2$ Systems

TiAl: In the coming year, we will examine the fatigue-crack growth behavior of ß-TiNb reinforced γ-TiAl intermetallic composites as a function of particle volume fraction, particle thickness and specimen orientation. In view of the susceptibility of the ductile TiNb ligaments to fatigue failure due to their low strain-hardening rate, studies will be extended to include other reinforcements such as Nb. More recent studies on TiAl intermetallics have shown that duplex (α_2 + γ) microstructures yield toughnesses in excess of 25 MPa$\sqrt{m}$; the effect of ductile-phase toughening on these TiAl microstructures will also be examined.

$MoSi_2$: In addition, we have received some Nb-reinforced and SiC-reinforced $MoSi_2$ composites from Dr. W. O. Soboyejo at McDonnell Douglas Research Laboratories and Dr. J. J. Petrovic at Los Alamos National Laboratory, respectively. Our research efforts will be directed at obtaining the R-curve and fatigue properties in these materials with emphasis on the mechanisms of crack extension. Our preliminary studies on Nb/$MoSi_2$ composites indicate that ductile-phase toughening may not be achieved, even under monotonic loading, because of the strong reaction layer interface between Nb and $MoSi_2$. The crack bows around the spherical Nb particles and does not sample the particle, to the effect that the toughness of $MoSi_2$ and Nb-reinforced $MoSi_2$ are nominally identical. Modifying the reaction layer through coating and the ductile-phase morphology in order that the crack traverses the particles may be alternatives for developing Nb/$MoSi_2$ composites with acceptable mechanical properties.

4.2 Nb_3Al and Nb_2Si Systems

Studies on the crack-growth behavior in Nb_3Al/Nb composites, both under monotonic and cyclic loading, will commence shortly. To date there are no data available on the mechanical performance of these materials. Of particular interest are the two microstructures (i) as hot pressed (at 1650°C) condition and (ii) following heat-treatment for 4 hrs at 1800°C, that yield Nb in two different morphologies in a Nb_3Al matrix with similar strength levels. Additionally, we will begin fabrication of niobium silicides by similar powder processing techniques.

5. ACKNOWLEDGEMENTS

This work was supported by the U.S. Air Force Office of Scientific Research under Grant No. AFOSR-90-0167, with Dr. A. H. Rosenstein as contract monitor. Professor G. R. Odette, who collaborates with us on TiNb/γ-TiAl intermetallic composites, is funded at the University of California at Santa Barbara by the Defense Advanced Projects Agency. Our thanks are due to Professor Odette, Dr. J. J. Petrovic at Los Alamos National Laboratory, Dr. W. O. Soboyejo at McDonnell Douglas Research Laboratories, Pratt and Whitney and Dr. R. H. Dauskardt for supplying the intermetallic composites and many helpful discussions.

6. PROGRAM ORGANIZATION AND PERSONNEL

The work described was performed in the Department of Materials Science and Mineral Engineering, University of California at Berkeley, under the supervision of Dr. R. O. Ritchie, Professor of Materials Science and Dr. L. C. De Jonghe, Professor of Materials Science, aided by a research engineer, graduate student research assistant and undergraduate research helpers. The individual personnel are listed below:

i) Professor R. O. Ritchie, Principal Investigator
(Department of Materials Science and Mineral Engineering)

ii) Professor L. C. De Jonghe, Co-Investigator
(Department of Materials Science and Mineral Engineering)

iii) Dr. K. T. Venkateswara Rao, Research Engineer
(Department of Materials Science and Mineral Engineering)

iv) L. Murugesh, Graduate Student Research Assistant
(Department of Materials Science and Mineral Engineering)

v) D. Nath, Undergraduate Engineering Aide
(Department of Mechanical Engineering)

vi) J. C. McNulty, Undergraduate Engineering Aide
(Department of Materials Science and Mineral Engineering)

7. PUBLICATIONS

7.1 Refereed Journals

1. K. T. Venkateswara Rao, G. R. Odette and R. O. Ritchie, "On the Contrasting Role of Ductile-Phase Reinforcements in the Fracture Toughness and Fatigue-Crack Propagation Behavior of TiNb/γ-TiAl Intermetallic-Matrix Composites," Acta Metallurgica et Materialia, 39 (1991), in press.

7.2 Conference Proceedings

2. K. T. Venkateswara Rao, G. R. Odette and R. O. Ritchie, "Fatigue and Fracture Resistance of Ductile-Phase Toughened Intermetallic-Matrix Composites: Behavior in ß-TiNb/γ-TiAl," in Fatigue of Advanced Materials, R. O. Ritchie, R. H. Dauskardt and B. N. Cox (eds.), Materials and Components Engineering Publications Ltd., Edgbaston, U.K. (1991), in press.

7.3 Invited Presentations

3. R. O. Ritchie, "Cyclic Behavior of Advanced Structural Materials," invited presentation to the DARPA Meeting on Fatigue and Reliability of Advanced Structural Materials, La Jolla, CA, July 1990.

4. R. O. Ritchie, "Fatigue of Advanced Materials," invited seminar to the Department of Materials Science and Mineral Engineering, University of California, Berkeley, CA, Sept. 1990.

5. K. T. Venkateswara Rao, R. O. Ritchie and G. R. Odette, "Failure Mechanisms in Ductile-Particle Toughened Intermetallic Composites: Behavior Under Monotonic vs. Cyclic Loading," Engineering Foundation Conference on Mechanical Fatigue of Advanced Materials, Santa Barbara, CA, January 1991.

6. K. T. Venkateswara Rao, G. R. Odette and R. O. Ritchie, "Ductile-Brittle Toughened Intermetallic-Matrix Composites: Fracture-Toughness vs. Fatigue-Crack Growth Behavior," invited talk to Symposium on Creep and Fatigue of Metal Matrix Composites, 1991 TMS Annual Spring Meeting, New Orleans, LA, February 1991.

7. K. T. Venkateswara Rao, S. C. Siu and R. O. Ritchie, "Role of SiC Fibers in Influencing the Monotonic and Cyclic Crack Growth in Continuously-Reinforced SiC_f/6061 Metal-Matrix Composites," 1991 TMS Annual Spring Meeting, New Orleans, LA, February 1991.

8. DISTRIBUTION LIST

AFOSR/NE
ATTN: Dr. A. H. Rosenstein
Bldg. #410
Bolling Air Force Base
Washington, D.C. 20332

AFWAL/MLLM
ATTN: Branch Chief
Wright-Patterson AFB
Dayton, OH 45433

AFWAL/MLLS
ATTN: Branch Chief
Wright-Patterson AFB
Dayton, OH 45433

AFWAL/MLLN
ATTN: Branch Chief
Wright-Patterson AFB
Dayton, OH 45433

Dr. Hugh R. Gray
NASA Lewis Research Center
Materials and Structures Division
21000 Brookpark Rd.
Cleveland, OH 44135